

Spectrum Syntheses of High Resolution Integrated Light Spectra of Galactic Globular Clusters^{*}

Charli M. Sakari^{1,5†}, Matthew Shetrone², Kim Venn¹, Andrew McWilliam³,
and Aaron Dotter⁴

¹*Department of Physics and Astronomy, University of Victoria, Victoria, BC V8W 3P2, Canada*

²*McDonald Observatory, University of Texas at Austin, HC75 Box 1337-MCD, Fort Davis, TX 79734, USA*

³*The Observatories of the Carnegie Institute of Washington, 813 Santa Barbara Street, Pasadena, CA 91101-1292, USA*

⁴*Research School of Astronomy and Astrophysics, The Australian National University, Weston, ACT 2611, Australia*

⁵*Vanier Canada Graduate Scholar*

4 April 2024

ABSTRACT

Spectrum syntheses for three elements (Mg, Na, and Eu) in high-resolution integrated light spectra of the Galactic globular clusters 47 Tuc, M3, M13, NGC 7006, and M15 are presented, along with calibration syntheses of the Solar and Arcturus spectra. Iron abundances in the target clusters are also derived from integrated light equivalent width analyses. Line profiles in the spectra of these five globular clusters are well fit after careful consideration of the atomic and molecular spectral features, providing levels of precision that are better than equivalent width analyses of the same integrated light spectra, and that are comparable to the precision in individual stellar analyses. The integrated light abundances from the 5528 and 5711 Å Mg I lines, the 6154 and 6160 Å Na I lines, and the 6645 Å Eu II line fall within the observed *ranges* from individual stars; however, these integrated light abundances do not always agree with the *average* literature abundances. Tests with the second parameter clusters M3, M13, and NGC 7006 show that assuming an incorrect horizontal branch morphology is likely to have only a small ($\lesssim 0.06$ dex) effect on these Mg, Na, and Eu abundances. These tests therefore show that integrated light spectrum syntheses can be applied to unresolved globular clusters over a wide range of metallicities and horizontal branch morphologies. Such high precision in integrated light spectrum syntheses is valuable for interpreting the chemical abundances of globular cluster systems around other galaxies.

Key words: Techniques: spectroscopic — globular clusters: individual(47 Tuc) — globular clusters: individual(M3) — globular clusters: individual(M13) — globular clusters: individual(NGC 7006) — globular clusters: individual(M15)

1 INTRODUCTION

Detailed chemical abundances from high-resolution spectroscopy of individual stars in globular clusters (GCs) associated with the Milky Way and its nearby satellite galaxies have provided valuable information about stellar evolution and nucleosynthesis (e.g., Gratton et al. 2004), the chemical evolution of low- and high-mass galaxies (e.g., Tolstoy et al. 2009), and the assembly history of the Milky Way (e.g., Freeman & Bland-Hawthorn 2002). In particular, chemical tagging has enabled the identification of potentially accreted stellar streams and GCs (e.g., Cohen 2004, Sbordone et al. 2005, Chou et al. 2010, Sakari et al. 2011), which shows that hierarchical merging has played an important role in the formation of the Milky Way Galaxy. Observations of extragalactic GC systems suggest that most galaxies have experienced complicated

assembly histories that may include a significant component of accretion from dwarf galaxies (see Harris 2000 and Brodie & Strader 2006 for reviews on the observed properties of GC systems). Certain models suggest that most GCs form in small dark matter halos at high redshift, and are accreted by larger galaxies at later times (Bekki et al. 2008; Muratov & Gnedin 2010). Detailed chemical abundances of extragalactic globular cluster systems, particularly those associated with galaxy types (e.g., massive ellipticals vs. spirals) and environments (e.g., located within galaxy clusters) that are not found in the Local Group, can provide information about the assembly histories of their host galaxies.

Individual stars are too faint for detailed spectral analyses beyond the Local Group. Distant extragalactic GCs, however, appear as bright, point-like sources, and can be observed at much greater distances than individual stars. Therefore, an alternative way to determine the flux-weighted average chemistry of a GC is from an integrated light spectrum (ILS) of the entire population. Informa-

† E-mail: sakariem@uvic.ca

tion on the chemical abundance ratios for a system of GCs can then be used to study the chemical evolution and early assembly history of the host galaxy. Integrated light spectroscopy has historically been done at low- to medium-resolution. Lower-resolution ILS analysis methods have been tested and calibrated on Galactic GCs within the last few decades (e.g., Schiavon et al. 2002; Lee & Worthey 2005)—such methods have proven capable of determining the ages, metallicities, and α -abundances of Galactic GCs. However, detailed abundances (of, e.g., iron-peak or neutron capture elements) require moving to higher resolution. By providing additional elements and higher precision, high resolution observations provide information about, for example, the contributions from different types of supernovae or AGB stars.

The high resolution integrated light abundance analysis program ILABUNDS (presented in McWilliam & Bernstein 2008, hereafter MB08), has been tested on several Galactic GCs. The majority of ILABUNDS analyses thus far have been equivalent width analyses, which are sufficient for elements with multiple, fairly strong lines since with a large number of lines the error in the mean abundance will be less sensitive to individual measurement errors. Equivalent width techniques have successfully reproduced the literature abundances (from individual stars) of α , iron peak, and neutron capture elements in several Galactic GCs (MB08, Cameron 2009) and produced reasonable abundances for inner halo M31 GCs, Large Magellanic Cloud GCs, and GCs associated with other Local Group dwarf galaxies (Colucci et al. 2009, 2011a,b, 2012). However, many elements do not have enough (or any) strong lines available for an *equivalent width* analysis. The features in ILS are also often weak and/or blended, which makes an *equivalent width* analysis particularly difficult. There are many elements with detectable spectral lines in high-resolution spectra, e.g., Cu, Zn, Ba, and Eu, which are valuable for galaxy and GC formation and chemical evolution theories (e.g., Matteucci et al. 1993, Mishenina et al. 2002, Travaglio et al. 2004) but which are unsuitable for an *equivalent width* analysis.

With individual stellar analyses, the preferred method for determining abundances of such elements is to *synthesize* the entire spectral region around the line of interest. This technique is different from an equivalent width analysis, because the line profile, width, and depth are fit simultaneously, while the effects of nearby lines are taken into account. When a line is too weak or a spectrum is too noisy, upper limits can be obtained with spectrum synthesis, which can still provide valuable constraints. Colucci et al. (2009, 2012) have synthesized high-resolution ILS to obtain abundances of Na, Mg, Al, Sr, Ba, La, and Eu, among other elements, with random 1σ errors that are typically on the order of 0.15 – 0.3 dex. These errors are quite large given the spectral resolution; lower uncertainties would be more useful for chemical comparisons between clusters or galaxies, or for comparisons with chemical evolution models. Tests on Galactic GCs can better determine the accuracy (through comparisons with literature abundances) and precision (through stringent tests on high S/N spectra) of integrated light spectrum syntheses.

In order to understand and quantify the accuracy and precision of an IL spectrum synthesis method, this paper presents tests on the five Galactic GCs 47 Tuc, M3, M13, NGC 7006, and M15 in four different 10 Å regions around the 5528 and 5711 Å Mg I lines, the 6154 and 6160 Å Na I lines, and the 6645 Å Eu II line. These elements have been selected because they are important for galaxy/GC formation theories. In addition, the lines are easily detectable in the majority of the spectra, providing abundances rather than upper limits. Other than the Eu II line, these lines and features

also avoid the complications of significant hyperfine structure or isotopic corrections.

The target clusters were selected to cover a range of metallicities and horizontal branch morphologies, as discussed in Section 2.1. Sections 2.2 and 2.3 describe the observations of these nearby targets, and the subsequent data reductions, while Section 3 describes the abundance analysis method used to infer the chemical abundances. The syntheses are finally presented in Section 4, along with detailed discussions of the errors. The important findings of this paper are discussed in Section 5. Finally, the results are summarized in Section 6.

2 OBSERVATIONS AND DATA REDUCTION

2.1 Target Selection

The targets were selected to span a range of metallicities (from $[\text{Fe}/\text{H}] = -0.7$ to -2.4) and HB morphologies (from red to very blue), though all appear to be standard Galactic GCs (i.e. old and α -enhanced). In particular, M3/M13/NGC 7006 form a “second parameter” triad, i.e. the three GCs have similar ages and metallicities, yet different HB morphologies. Basic information about the target clusters is provided in Table 1. Positions and integrated V magnitudes are from Harris (1996; 2010 edition); the $[\text{Fe}/\text{H}]$, $[\alpha/\text{Fe}]$, and age estimates come from isochrone fits by Dotter et al. (2010, 2011); and the horizontal branch (HB) index, $(B - R) / (B + V + R)$, (where B , R , and V are the number of stars blueward, redward, and inside of the instability strip) comes from Mackey & van den Bergh (2005). In order to minimize the uncertainties that occur when modeling the stellar populations, resolved photometry was utilized to estimate atmospheric parameters for the GC stars (see Section 3.1.1).

2.2 Observations

The 47 Tuc spectrum was kindly provided by R. Bernstein & A. McWilliam. It is the same spectrum analyzed in MB08; details on the observations and data reduction can be found there. Additional normalizations with low-order polynomials were performed and the apertures were combined, as described below.

The other spectra were observed with the High Resolution Spectrograph (HRS; Tull 1998) on the Hobby-Eberly Telescope (HET; Ramsey et al. 1998; Shetrone et al. 2007) at McDonald Observatory in Fort Davis, TX in 2011 and 2012. A slit width of $1''$ was used, leading to an instrumental spectral resolution of $R \approx 30,000$. Given the velocity dispersions of the targets (see below), a higher spectral resolution is unnecessary. The 600 gr/mm cross disperser was used, with a central wavelength of 6302.9 Å. The spectral coverage is therefore $\sim 5320 - 6290$ Å on the blue chip and $\sim 6360 - 7340$ Å on the red chip. This wavelength range was chosen for future unresolved targets in order to minimize the effects of improperly modeled HBs, since blue HB stars should contribute less to the integrated light at red wavelengths.

ILS observations of distant, point-like targets are relatively simple. Nearby GCs, however, are much more difficult to observe for integrated light studies, given their large sizes on the sky and the fact that their stars *are* resolved. It is essential to observe these difficult targets, however, because the ILS methods can be calibrated through comparisons with abundances from individual stars. To overcome these observational difficulties, the ILS of M3, M13, NGC 7006, and M15 were obtained by scanning the HRS fibers

Table 1. The target clusters.

Cluster	RA (J2000)	Dec (J2000)	V_{int}	[Fe/H]	[α /Fe]	Age	HB index
47 Tuc (NGC 104)	00 ^h 24 ^m 05 ^s .67	-72°04'52".6	3.95	-0.70	0.2	12.75 ± 0.50	-0.99
M3 (NGC 5272)	13 ^h 42 ^m 11 ^s .62	+28°22'38".2	6.19	-1.60	0.2	12.50 ± 0.50	0.08
M13 (NGC 6205)	16 ^h 41 ^m 41 ^s .24	+36°27'35".5	5.78	-1.60	0.2	13.00 ± 0.50	0.97
NGC 7006	21 ^h 01 ^m 29 ^s .38	+16°11'14".4	10.56	-1.50	0.2	12.25 ± 0.75	-0.28
M15 (NGC 7078)	21 ^h 29 ^m 58 ^s .33	+12°10'01".2	6.20	-2.40	0.2	13.25 ± 1.00	0.67

References: Positions and integrated magnitudes are from Harris (1996; 2010 edition). The [Fe/H], [α /Fe], and age estimates are from isochrone fitting (Dotter et al. 2010, 2011). The HB index, $(B - R) / (B + V + R)$, comes from Mackey & van den Bergh (2005).

across the cluster cores. A number of specific pointings on the cluster were selected, and the fibers were moved to each position. The large 3'' fiber was used in order to maximize spatial coverage on the clusters. HRS provides two additional 3'' fibers located 10'' from the center of the object fiber. In typical observations these extra fibers are intended to serve as sky fibers; however, because of the spatial extent of the Galactic GCs, these sky fibers served as additional object fibers during the observations. Separate sky observations with all three fibers were therefore taken after each GC observation. These pointing patterns are shown in Figure 1, along with the clusters' core and half-light radii.

For M3, M13, and NGC 7006, the entire core of each cluster was observed, though the clusters were too large to observe the entire area within the half-light radius in a reasonable amount of time. Note that M15 was mapped differently than NGC 7006, M3, or M13; its wedge-shaped map represents a slice of the cluster out to the half-light radius, assuming the cluster is spherically symmetric. Any differences in the spectra as a result of the different mappings will be negligible because the input photometry have been selected to reflect the spatial coverage of the ILS (see Section 3.1.1).

The total exposure times and S/N ratios in blue (5500 Å) and red (7000 Å) regions are shown in Table 2. Generally, the exposure times were calculated to allow an observation of a single HB star to reach S/N = 70, though NGC 7006 did not receive sufficient time to meet this goal.

2.3 Data Reduction

The data reduction was performed in the Image Reduction and Analysis Facility program (IRAF)¹ according to the standard HRS data reduction methods, with several exceptions. A separate bias frame removal was not completed, as the process can add noise to the spectra.² To remove cosmic rays the aperture extraction was performed with variance weighting, where IRAF considers the gain and read noise of the CCD and identifies and removes any pixels that deviate significantly from the noise. This variance weighting procedure occasionally affects the shape of the continuum; thus, the shape of the non-weighted extraction was maintained.

Separate sky observations were obtained after all ILS observations. Again, all three fibers (object and sky) were used in each exposure; the spectra from the three fibers were averaged together

to remove noise and cosmic rays. Because the sky spectra were still fairly noisy, the spectra were replaced with continuum fits and the emission lines were added back in (using the sky line identifications from the UVES Quality Control sky spectrum website³). The IRAF task *skytwavek* determined the necessary scaling factor between a target object spectrum and its sky spectrum, and the sky spectrum was multiplied by that factor before it was subtracted from the object spectrum. Telluric standards were also observed during each night, allowing separate removal of the telluric absorption lines.

Because ILS may have many undetectable, blended, weak features that can obscure/distort the continuum level, the spectra must be carefully normalized. To remove the blaze function of the spectrograph and the blackbody function of the cluster, an extremely metal-poor (EMP) giant was observed with the same instrumental setup. An EMP star should have very few spectral lines, and finding the continuum should therefore be quite simple. Furthermore, an EMP giant should have a similar effective temperature as the average temperature of the cluster. Information on the observed EMP star, CS29502-092, is given in Table 3. The EMP star's continuum was fit with the IRAF task *continuum*, and the target spectra were divided by these continuum fits. Additional low-order polynomial fits were required to fully normalize the target spectra.

The normalized GC spectra were then cross-correlated with a reference spectrum (using the IRAF task *fxcor*) to determine the radial velocity and velocity dispersion. Arcturus was used as the template spectrum for the cross-correlation; this very high resolution ($R = 150,000$) spectrum was observed with the Fourier Transform Spectrometer (FTS) on the McMath Telescope (Hinkle 2003), and was obtained from the Arcturus Atlas.⁴ The IRAF task *fxcor* correlates the target spectra with the Arcturus template spectrum, and identifies the values with the highest correlation; the peak of the correlation occurs at the observed radial velocity of the cluster, and the width determines the velocity dispersion (as discussed below). The heliocentric velocities were measured from each observation, and were averaged together to produce the final, averaged heliocentric velocities (shown in Table 2).

Each of the individual reduced and normalized spectra were shifted to the rest frame, using the radial velocity from *fxcor*. The rest frame spectra were then combined with average sigma-clipping rejection routines. The individual observations were weighted by flux during the averaging. The blue ends of the individual apertures often suffered from lower S/N, especially at blue wavelengths. These noisy regions were removed from the spectrum before the individual apertures were combined. Examples of the final spectra are shown in Figure 2, along with notable spectral features.

¹ IRAF is distributed by the National Optical Astronomy Observatory, which is operated by the Association of Universities for Research in Astronomy, Inc., under cooperative agreement with the National Science Foundation.

² In addition, the scattered light subtraction removes some of the bias level; see the online HRS Data Reduction Tips at <http://hydra.as.utexas.edu/?a=help&h=29#HRS>

³ http://www.eso.org/observing/dfo/quality/UVES/pipeline/sky_spectrum.html

⁴ <ftp://ftp.noao.edu/catalogs/arcturusatlas/>

Table 2. GC observations.

Cluster	Observation Dates	Exposure Time (s)	S/N ^a (5500 Å)	S/N ^a (7000 Å)	$v_{\text{helio,obs}}$ (km/s)	$v_{\text{helio,lit}}$ (km/s)	σ_{obs} (km/s)	σ_{lit} (km/s)
47 Tuc ^b	2000 Jul 18, 19	11030	120	180	-	-	11.50 ± 0.30^c	11.0
M3	2012 Mar 25, Apr 16, 17, 18	9940	180	230	-146.0 ± 1.1	-147.6	5.66 ± 0.15	5.5
M13	2012 Apr 17, 20, 22	11569	130	250	-247.5 ± 1.3	-244.2	7.23 ± 0.33	7.1
NGC 7006	2011 Sep 24, 2012 May 29, Jun 19	8903	65	130	-380.4 ± 0.7	-384.1	4.49 ± 0.60	-
M15	2011 Sep 27	3280	95	220	-106.6 ± 0.2	-107.0	12.54 ± 0.60	13.5

References: Literature values are from the Harris Catalog (Harris 1996; 2010 edition).

^aS/N ratios (per pixel) are measured in IRAF.

^b47 Tuc was observed with the Las Campanas 2.5 m Du Pont Telescope by R. Bernstein & A. McWilliam; see MB08 for more details.

^cThis velocity dispersion has been determined in the same way as the other GCs, for consistency.

Table 3. Properties of the observed EMP star.

Star	RA (J2000)	Dec (J2000)	V	T_{eff} (K)	Observation Dates	Exposure Times (s)	S/N ^a (5500 Å)	S/N ^a (7000 Å)	v_{helio}^b (km/s)
CS29502-092	22 ^h 22 ^m 36 ^s .0	-01°38′27″.5	11.87	5001	2011 Nov 16	690	167	341	-67.0 ± 0.4

References: The position and magnitude are from the SIMBAD database. The stellar temperature is an average from the Stellar Abundances for Galactic Archaeology (SAGA) database (Suda et al. 2008).

^aS/N ratios (per pixel) are measured in IRAF.

^bThe radial velocity was determined in the same way as the GC targets.

After the individual observations were combined, the final spectra were again cross-correlated with Arcturus to determine the cluster velocity dispersions. The width of the cross-correlation peak in *fxcor* depends on the width of the spectral lines. In individual stars the line width is often dominated by the instrumental broadening, though rotation, microturbulence, etc. can also affect the line width. In an ILS, the velocity dispersion of the target is often the dominant source of broadening. The full-width at half maximum (FWHM) of the cross-correlation peak of an ILS is therefore related to the velocity dispersion, σ , of the cluster, as described by Alpaslan (2009). Since the instrumental broadening is still significant in the target GCs,⁵ the observed velocity dispersion is found by subtracting (in quadrature) the instrumental broadening. The broadening of the target spectrum is taken into account in the calibration curve, though there may be additional sources of broadening that are unaccounted for. Thus, the derived velocity dispersions may be upper limits. This is not crucial for this analysis, since only the total width of the lines is important. These velocity dispersions for the target GCs are reported in Table 2, and are in good agreement with the literature values. Line blends in the ILS may lead to overestimates of the velocity dispersion; however, this does not seem to be significant for these GCs.

⁵ Recall that $R = 30,000$, which means that the FWHM from instrumental broadening alone should be 10 km/s. This instrumental broadening is likely to vary across the CCD—however, these variations are likely to be insignificant in ILS given the width of the lines.

2.4 Calibration Spectra

As shown in Section 4, the success of spectrum synthesis relies upon a complete and accurate input line list. To test the accuracy of these input line lists, spectrum syntheses of the Solar and Arcturus spectra have been performed. The Solar spectrum ($R = 300,000$; Kurucz 2005) comes from the Kurucz 2005 solar flux atlas.⁶ Solar atmospheric parameters of $T_{\text{eff}} = 5777$ K, $\log g = 4.44$ dex, $\chi = 0.85$ km s⁻¹, and $[M/H] = 0.0$ were adopted (Yong et al. 2005).

The Arcturus spectrum is the same one used for the cross-correlation with the target ILS (see Section 2.3). Arcturus atmospheric parameters of $T_{\text{eff}} = 4300$ K, $\log g = 1.50$ dex, $\chi = 1.56$ km s⁻¹, and $[M/H] = -0.6$ (Yong et al. 2005) were adopted. This Arcturus temperature and surface gravity are in excellent agreement with Fulbright et al. (2006) and Ramírez & Allende Prieto (2011), though the microturbulence values and metallicities differ slightly between the three studies. Both Fulbright et al. (2006) and Ramírez & Allende Prieto (2011) find higher metallicities and microturbulence values, with $\xi = 1.67$ km s⁻¹ and $[Fe/H] = -0.50$, and $\xi = 1.74$ km s⁻¹ and $[Fe/H] = -0.52$, respectively. The Yong et al. microturbulence and metallicity are adopted here, because their values agree best with the Fe I and Fe II abundances derived in this work (Section 3.1.3).

⁶ <http://kurucz.harvard.edu/sun.html>

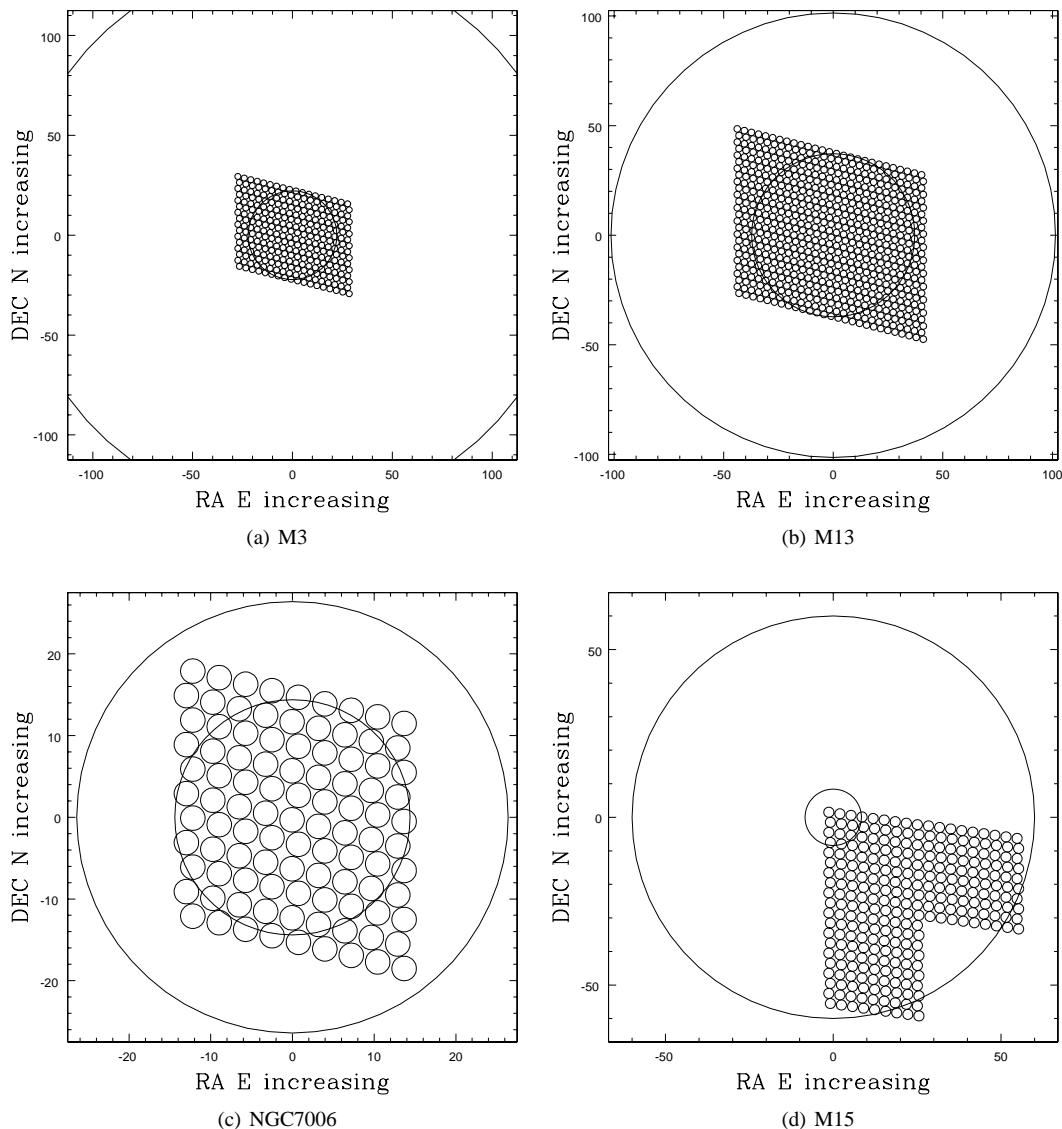


Figure 1. Fiber pointings for the HET observations of the target clusters. The small circles show the positions of the 3'' fibers (both sky and object), while the larger circles show the core and half-light radii (from Harris 1996; 2010 edition). The centers of the clusters are shown at arbitrary positions. Each observation scans the three fibers across the cluster; for an individual GC, each pointing lasts for the same amount of time, and the pointings are not overlapped.

3 DETAILED ABUNDANCES WITH ILABUNDS

The chemical abundances in the target GCs were determined with the program ILABUNDS (MB08). ILABUNDS is a modification of the 1997 version of the local thermodynamic equilibrium (LTE) line analysis and spectrum synthesis code MOOG⁷ (Snedden 1973). The equivalent width version of ILABUNDS was described and presented in MB08; here, a spectrum synthesis version of ILABUNDS (recently developed by A. McWilliam) is employed.

For spectrum syntheses of individual stars, MOOG requires an input model atmosphere and line list. ILABUNDS operates similarly, except that a model atmosphere must be provided for each star in the cluster, and the line list must be fairly complete. The input model atmospheres for ILABUNDS are discussed in Section

3.1, while the input line list is discussed in Section 3.2. With these inputs, the spectrum synthesis code calculates a synthetic ILS for each population box (Section 3.1.2) and combines the spectra together, weighted by flux. The final synthetic spectrum is broadened by the instrumental broadening and velocity dispersion (see Section 2.3), and is compared to the observed spectrum.

3.1 Model Atmospheres

For each star observed in the ILS the atmospheric parameters (effective temperature, T_{eff} ; surface gravity, $\log g$; microturbulence, ξ ; and metallicity, $[\text{Fe}/\text{H}]$) must be known in order to determine a cluster's integrated light chemical abundances. The stellar temperature, gravity, and microturbulence values are estimated from observed photometry (Section 3.1.1), which is grouped into color-magnitude diagram (CMD) boxes to simplify the process (Section

⁷ <http://www.as.utexas.edu/~chris/moog.html>

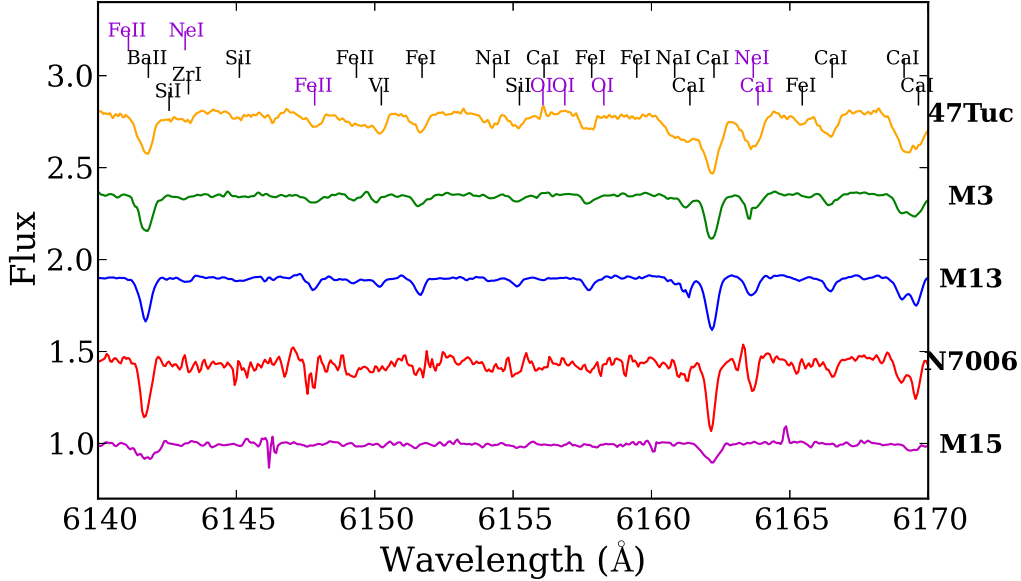


Figure 2. The ILS of the five Galactic GCs studied in this work. The 47 Tuc spectrum is from MB08, while the other four are HET spectra. Lines of interest are noted; the lines identified in black are lines that are typically used in standard RGB stellar analyses, while those in purple are used with hotter stars. The differences in line strengths are due to population, composition, and velocity dispersion differences between the five GCs.

3.1.2). The metallicities are found through a standard ILS equivalent width analysis (Section 3.1.3). Once the atmospheric parameters of a CMD box are known, a corresponding model atmosphere (from the Kurucz database;⁸ Castelli & Kurucz 2004) is then assigned.

3.1.1 Input Photometry

For unresolved targets the atmospheric parameters of the stars in a cluster must be modeled with isochrones, and observational diagnostics must be developed in order to ensure that the population is correctly modeled (see, e.g., Colucci et al. 2009, 2011a). With nearby targets, the uncertainties from modeling the stellar populations can be removed with the use of resolved photometry, which provides the color and magnitude of each star in the observed region. These observable quantities are then converted to physical quantities via empirical relations.

For 47 Tuc, the Hubble Space Telescope (HST) B , V data from R. Schiavon (Guhathakurta et al. 1992; Howell et al. 2000) were used to estimate the stellar parameters—more information on this data can be found in MB08. For M3, M13, NGC 7006, and M15, the V , I HST photometry from the ACS Galactic Globular Cluster Survey (e.g. Sarajedini et al. 2007; Anderson et al. 2008; Dotter et al. 2011) provided the estimates for the stellar atmospheric parameters. The $(m - M)_V$ and $E(B - V)$ values from Harris (1996; 2010 edition), the $E(V - I)$ extinction corrections of McCall (2004), and the $(V - I)$ color-temperature conversions from Ramírez & Melendez (2005) then provided the temperatures and surface gravities of the stars, as described in MB08. For stars that fell outside the Ramírez & Melendez (2005) calibration space, the atmospheric parameters of the Kurucz models that best matched

the observed values were adopted. An empirical relationship between the surface gravity and the microturbulence (also described in MB08) provided values for ξ .

The input photometry does not *exactly* match the populations observed in the ILS. Although the photometry were selected to only include stars within the maximum radii covered by the HET, the non-circular coverage of the ILS introduces some population differences (particularly for M15; see Figure 1). Field star contamination may also affect the input photometry and the observed spectrum. The presence of even one additional bright star can affect the observed ILS and the subsequent analysis (for example, the bright blue star in NGC 7006’s CMD). The effects of stochastic sampling of the brightest stars in unresolved targets have been investigated by Colucci et al. (2011a), who used Monte Carlo sampling to populate their stellar populations. They found, for an old, metal-poor GC, that the maximum difference in $[\text{Fe}/\text{H}]$ is only ~ 0.08 dex when randomly repopulating the entire GC. Resolved Galactic GCs with HST photometry provide a unique opportunity to test these results directly. For example, ILS of different scanned areas of the clusters can be compared (e.g., different wedges of M15), or test stars can be artificially added to the input photometry. These latter tests will be discussed in a subsequent paper (Sakari et al., in prep.), though preliminary syntheses of the lines presented in this paper suggest that field stars are unlikely to have a significant effect on the synthesized abundances. In particular, if the bright blue star in NGC 7006’s CMD were a Solar metallicity field star with slow rotation, several sharp features would be present in the observed ILS; however, these sharp features are not observed, and they would have a negligible effect on the final abundances.

3.1.2 CMD Boxes

The process of assigning model atmospheres is simplified by binning the stars together into boxes, based on their position in the

⁸ <http://kurucz.harvard.edu/grids.html>

CMD. Each CMD box is then assigned a model atmosphere with the average color, magnitude, temperature, etc. of all the stars in the box; the contributions to the total ILS from each box are then weighted by the number of stars in each box.

The CMD boxes for M3, M13, NGC 7006, and M15 are shown in Figure 3, while Tables 4 through 7 list the characteristics of these population boxes (see MB08 for a figure and list of the 47 Tuc boxes). The stars are boxed in approximately the same way as 47 Tuc, i.e., the number of red giant branch and main sequence boxes is approximately the same, and the coarseness of the boxes increases down the RGB. The number of boxes on the HB differ between the clusters as a result of the different HB morphologies. A forthcoming paper (Sakari et al., in prep.) shows that redefining the boxes has a negligible effect on the output abundances. The approximate evolutionary stages for each box are also shown in Tables 4 through 7, while the 50% V magnitude light levels are indicated by dashed lines in Figure 3. This shows that the brightest red giants, asymptotic giant branch stars, and HB stars truly do dominate the V -band flux.

The number of stars drops slightly in the lower main sequence boxes. This may be due to a combination of photometric incompleteness and mass segregation. Increasing the number of stars in the faintest two boxes has an insignificant effect on the abundances, suggesting that this effect can be neglected.

3.1.3 Metallicities

The iron abundances were determined through an integrated light equivalent width (EW) analysis, as described in MB08. The EWs were measured with a modified version of the automated program DAOSPEC⁹ (Stetson & Pancino 2008), as described below. The Fe lines used in the analysis, the atomic data, and the measured EWs (in the Sun, Arcturus, and the target GCs) are shown in Table 8. These lines are from the ILS line lists in MB08 and Colucci et al. (2009), with additional RGB lines from Sakari et al. (2011) and Venn et al. (2012). Note that the lines were restricted to the wavelength region covered by the HET spectra—thus, 47 Tuc has fewer lines than in MB08. Lines stronger than 150 mÅ were not included in the Fe abundance analysis (see McWilliam et al. 1995b).

3.1.3.1 DAOSPEC and ILS DAOSPEC is intended for high resolution ($R > 15000$), high SNR (> 30) spectra (Stetson & Pancino 2008); to our knowledge, this is its first application to ILS. The program iteratively fits a continuum to the input spectrum, detects the spectral lines in a defined region, and fits Gaussian profiles to the lines, providing their EWs. One major advantage of DAOSPEC over hand-measurements with IRAF's *splot* is the enforcement of a fixed full-width at half maximum (FWHM) for all lines.¹⁰ In individual stars, the FWHM is often dominated by the instrumental broadening of the spectrograph; in ILS, however, the velocity dispersion often dominates the line FWHM, blending together many of the spectral lines. To ensure that DAOSPEC can detect these features, the program was modified to detect lines that are separated

by a least half of a FWHM (rather than the default separation of one FWHM).

The success of DAOSPEC seems highly dependent on the choice of input parameters, at least for ILS. DAOSPEC has the option to determine its own FWHM. However, because ILS contain so many weak and/or blended features, the FWHM was fixed to the input parameter. This input FWHM is the sum (in quadrature) of the broadening from the velocity dispersion, the spectrograph, and the intrinsic broadening of Arcturus (see Section 2.3), and is given in pixels. This FWHM was then allowed to scale with wavelength. Another important input is the order of the polynomial-fit to the continuum. For individual stars, Stetson & Pancino (2008) found that higher-order continuum fits produced the best results. Again, however, ILS suffer from contributions from a variety of stars, severe blends, and line blanketing; high-order fits could therefore remove real features from the spectra, leading to underestimates of the line strengths. As described in Section 2, the HET spectra presented here have been carefully and conservatively normalized—thus the continuum was unchanged from the input. Occasionally valuable lines were mis-measured by DAOSPEC; these lines were re-measured with Gaussian fits in IRAF's *splot* task.

Previous tests have shown that with the correct input parameters DAOSPEC is capable of reproducing *splot*-measured EWs (in IRAF) for individual stars (Stetson & Pancino 2008; Sakari et al. 2011). DAOSPEC is also capable of reproducing *splot* EWs in the ILS of 47 Tuc. Figure 4a shows that for Fe lines the agreement between DAOSPEC and *splot* EWs is excellent, with an average offset of only 1.76 mÅ, though the scatter about the average is significant (± 9.93 mÅ). This scatter is likely caused by blends in the ILS, which can be difficult to detect by eye. DAOSPEC also reproduces the EWs of MB08, which were measured with the program GETJOB (McWilliam et al. 1995a). The offset between the datasets remains insignificant (0.37 mÅ, with the DAOSPEC EWs slightly higher), and the scatter is smaller (± 6.69 mÅ). Note that MB08 did not combine their apertures; the spectral lines in the overlapping regions were measured twice, and both measurements were included in their analysis. For this EW comparison the two EWs were averaged together for all lines in the overlapping regions. In individual stars, DAOSPEC often underestimates the EWs of the strongest lines (e.g. Sakari et al. 2011)—thus, the EWs of these lines have been verified or corrected in *splot*.

DAOSPEC is therefore capable of accurately reproducing the EWs of the lines in the 47 Tuc ILS. Since 47 Tuc has a higher velocity dispersion than most of the targets in this work (except for M15; see Table 2), DAOSPEC should also be able to accurately measure the EWs for all the target GCs. However, care must be taken with the strongest lines, to ensure they are properly measured, and attention must be paid to lines in regions with uncertain continuum normalization.

3.1.3.2 Fe abundances The Fe I and Fe II EWs for the target GCs were input into ILABUNDS, along with the model atmospheres derived from the HST photometry. The [Fe/H] values for each line were computed differentially (i.e. relative to the derived Solar abundance *for that line*), in order to reduce uncertainties from, e.g., atomic data. If the Solar lines were stronger than $\text{EW} \gtrsim 200$ mÅ, a value of $\log \epsilon_{\text{Fe}, \odot} = 7.50$ (Asplund et al. 2009) was instead adopted. The average [Fe I/H] and [Fe II/H] ratios for Arcturus and the target GCs are shown in Table 9. Also shown are the uncertainties in the average Fe abundances, as determined from the line-to-line scatter, σ , divided by \sqrt{N} , where N is the number of lines. Since only a single line is available for M15's Fe II abun-

⁹ DAOSPEC has been written by P.B. Stetson for the Dominion Astrophysical Observatory of the Herzberg Institute of Astrophysics, National Research Council, Canada.

¹⁰ Though of course this fixed FWHM, $\Delta\lambda$, is allowed to scale appropriately with wavelength, given the constant resolving power of the spectrum, $R = \lambda/\Delta\lambda$.

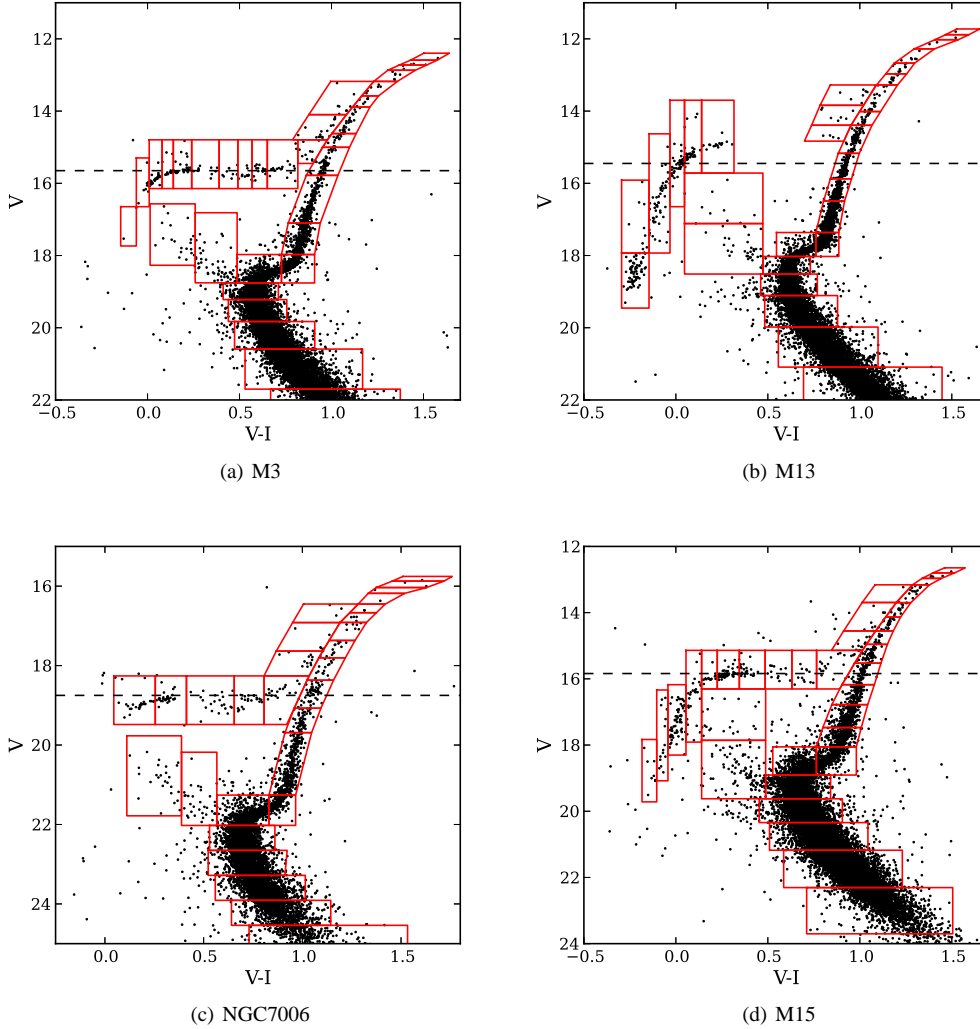


Figure 3. Johnson’s V , I CMDs of the target clusters, from HST (Sarajedini et al. 2007; Anderson et al. 2008; Dotter et al. 2010, 2011). The stars have been selected based on their distances from the cluster center, to reflect the populations sampled by the ILS. Overlaid are the boxes used to assign model atmospheres to the stars. The 50% V -band light levels are shown by the horizontal dashed lines. The brightest stars that lay outside the boxes may be field stars—the possible effects of these field stars will be investigated in a future paper, but are not likely to have significant effect on the syntheses presented here.

dance, the Cayrel (1988) formula was used to determine the error in the Fe II line’s EW, as described in Sakari et al. (2011). The adopted uncertainty in abundance was then found by rerunning IL-ABUNDS with the new EWs.

As stated earlier, the Arcturus values agree well with Yong et al. (2005). The GC [Fe/H] values in Table 9 agree quite well with the literature values quoted in Harris (1996; 2010 edition), which are also shown in Table 9. The 47 Tuc integrated light [Fe I/H] values are slightly different from the ILS values from MB08 (which are also shown in Table 9), though the 47 Tuc integrated light [Fe II/H] ratios are in excellent agreement with MB08. Given that the EWs (Figure 4b) and CMD boxes are nearly identical, and since both [Fe I/H] ratios have been computed differentially, it is puzzling that the [Fe I/H] values are not in agreement. The two $\log \epsilon_{\text{Fe}}$ values are actually in agreement ($\log \epsilon_{\text{Fe}} = 6.73$ compared to MB08’s 6.77)—this suggests that there are differences in how the differential ratios are computed.

For the remainder of this paper, all quoted [X/Fe] values are computed with the integrated light Fe abundances derived here.

3.1.4 Hot Stars

Stars hotter than ~ 8000 K are expected to show chemical abundance variations as a result of radiative levitation which may bring the hottest stars up to Solar composition (e.g. Behr et al. 2000; Behr 2003; Lovisi et al. 2012). To test this result, syntheses of M13 were completed with Solar composition hot stars. These tests are discussed in more detail in a forthcoming paper; here it is simply noted that these abundance variations have a negligible effect on the syntheses of the lines studied here.

Hot stars have also been observed to have large rotational velocities (up to ~ 60 km/s; Behr 2003). Syntheses were also performed on M13, assuming all stars hotter than 8000 K have Solar composition *and* rotational velocities of $v \sin i = 60$ km/s. The effects are again negligible, since the increased broadening weakens

Table 4. M3's CMD Boxes

	$V_{0,\text{avg}}$	$(V - I)_{0,\text{avg}}$	T_{eff} (K)	$\log g$	ξ (km/s)	R (R_{\odot})	$f(V)$	N
RGB	12.502	1.564	3995	0.333	1.87	100.95	0.0141	1
	12.675	1.450	4125	0.517	1.83	81.63	0.0361	3
	12.754	1.377	4218	0.627	1.81	71.90	0.0224	2
	12.981	1.334	4266	0.759	1.78	61.81	0.0544	6
	13.332	1.218	4437	1.023	1.73	45.60	0.0394	6
	13.683	1.164	4521	1.220	1.69	36.34	0.0332	7
	14.270	1.081	4676	1.547	1.62	24.94	0.0761	28
	14.748	1.014	4686	1.745	1.57	19.86	0.0284	16
	15.398	0.952	4810	2.072	1.50	13.63	0.0712	74
	16.446	0.879	4975	2.575	1.40	7.64	0.0695	197
SGB	17.470	0.824	5114	3.047	1.30	4.43	0.0419	296
	18.185	0.769	5265	3.400	1.22	2.96	0.0252	338
MS	18.512	0.619	6166	3.850	1.13	1.76	0.0530	960
	18.959	0.568	6403	4.098	1.07	1.32	0.0630	1720
	19.475	0.588	6336	4.283	1.03	1.07	0.0707	3120
	20.147	0.651	6075	4.472	0.99	0.86	0.0552	4557
	20.992	0.773	5586	4.647	0.96	0.70	0.0323	5928
AGB/HB	22.113	0.999	4716	4.700	0.94	0.66	0.0067	3549
	13.697	1.052	4757	1.364	1.65	30.79	0.0363	8
	14.471	0.948	4820	1.707	1.58	20.75	0.0362	16
	15.084	0.861	5018	2.051	1.51	13.96	0.0129	10
	15.468	0.733	5374	2.360	1.44	9.78	0.0170	19
	15.615	0.599	5855	2.599	1.39	7.43	0.0144	18
	15.718	0.521	6438	2.829	1.34	5.70	0.0080	11
	15.654	0.436	6773	2.902	1.33	5.24	0.0069	9
	15.610	0.292	7360	3.043	1.30	4.46	0.0097	12
	15.481	0.179	7886	3.110	1.28	4.13	0.0267	30
BS	15.529	0.103	8372	3.217	1.26	3.65	0.0111	13
	15.834	0.028	9168	3.450	1.21	2.79	0.0163	25
	15.953	-0.021	10189	3.584	1.18	2.39	0.0045	8
	17.501	-0.144	15471	4.506	0.99	0.83	0.0001	1
	18.145	0.355	7309	4.022	1.09	1.44	0.0042	57
	17.356	0.146	8264	3.922	1.11	1.62	0.0030	20

The average V and $(V - I)$ colors of each box are shown, along with the average effective temperature, surface gravity, microturbulence, radius, fractional V -band flux, and number of stars assigned to each box. The different evolutionary stages of the boxes are also shown, where RGB stands for Red Giant Branch, SGB for Subgiant Branch, MS for Main Sequence, AGB for Asymptotic Giant Branch, HB for Horizontal Branch, and BS for Blue Stragglers. Note that the 50% light level for M3 is $V_{1/2} = 15.65$, which reaches the middle of the HB.

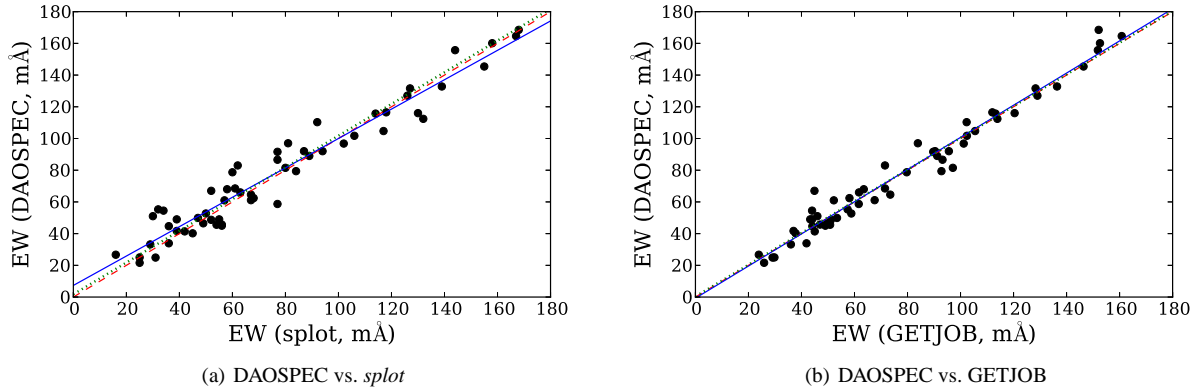


Figure 4. Comparisons of EW measurements on the ILS of 47 Tuc for the Fe lines in common between the studies. Figure 4a compares the DAOSPEC measurements to those from *splot*, while Figure 4b compares measurements from DAOSPEC and GETJOB (from MB08). Each black point is a separate spectral line. The dashed red lines show perfect agreement, while the dotted green lines show the average offset. The solid blue lines are linear least squares fits to the points. The agreement is excellent in both cases.

Table 5. M13's CMD Boxes

	$V_{0,\text{avg}}$	$(V - I)_{0,\text{avg}}$	T_{eff} (K)	$\log g$	ξ (km/s)	R (R_{\odot})	$f(V)$	N	
RGB	11.739	1.494	4083.	0.400	1.86	93.39	0.0158	1	
	11.907	1.494	4070.	0.458	1.85	87.35	0.0136	1	
	12.059	1.373	4221.	0.649	1.81	70.16	0.0236	2	
	12.474	1.257	4377.	0.933	1.75	50.57	0.0561	7	
	12.740	1.192	4477.	1.110	1.71	41.23	0.0565	9	
	13.035	1.155	4541.	1.269	1.67	34.36	0.0526	11	
	13.601	1.061	4717.	1.600	1.60	23.46	0.0556	20	
	14.123	1.003	4707.	1.803	1.56	18.58	0.0350	20	
	14.681	0.952	4809.	2.081	1.50	13.48	0.0808	78	
	15.469	0.890	4948.	2.467	1.42	8.65	0.0506	101	
	16.134	0.852	5040.	2.776	1.35	6.06	0.0369	135	
	16.839	0.816	5133.	3.100	1.29	4.17	0.0486	346	
	SGB	17.525	0.779	5247.	3.424	1.22	2.87	0.0196	257
		17.809	0.662	5987.	3.808	1.13	1.85	0.0357	608
	MS	18.213	0.585	6329.	4.074	1.08	1.36	0.0677	1676
		18.738	0.580	6369.	4.295	1.03	1.05	0.0805	3249
19.441		0.635	6146.	4.507	0.99	0.83	0.0812	6352	
20.367		0.762	5633.	4.710	0.94	0.65	0.0478	8903	
21.594		1.007	4699.	4.778	0.93	0.60	0.0158	9561	
AGB	13.473	0.969	4776.	1.581	1.61	23.99	0.0223	7	
	14.022	0.841	5069.	1.947	1.53	15.74	0.0134	7	
	14.646	0.817	5133.	2.224	1.47	11.43	0.0044	4	
HB	14.851	0.194	7816.	3.139	1.28	3.99	0.0153	17	
	14.879	0.054	8836.	3.322	1.24	3.23	0.0261	32	
	15.389	-0.013	9951.	3.649	1.17	2.22	0.0247	46	
	16.169	-0.105	13400.	4.157	1.06	1.24	0.0122	53	
	16.745	-0.214	20818.	4.733	0.94	0.64	0.0013	10	
BS	18.333	-0.247	24467.	5.000	0.78	0.27	0.0024	67	
	16.465	0.193	7980.	3.809	1.13	1.85	0.0019	10	
	17.656	0.341	7408.	4.144	1.06	1.25	0.0022	34	

The 50% light level for M13 is $V_{1/2} = 15.45$, which is slightly below the reddest HB stars.

the line strengths in HB stars. The changes in composition and the high rotation of HB stars are therefore ignored in this analysis.

3.2 Input Line Lists

To demonstrate the necessity of having a complete, calibrated line list, spectrum syntheses were performed with three different line lists.

Minimal List: This list uses only lines found in standard RGB equivalent width analyses. The ILS-specific line lists from MB08 and Colucci et al. (2009) were supplemented with additional RGB lines (from the line lists assembled in Sakari et al. 2011 and Venn et al. 2012.)

VALD List: This list consists of RGB lines from the Vienna Atomic Line Database¹¹ (VALD; Kupka et al. 2000). These are lines that VALD has determined would appear (to at least 2%) in a tip of the RGB star at 47 Tuc's metallicity. None of the atomic data were changed from the VALD values.

Final List: The Final Line List consists of lines from the Minimal List, with supplements from VALD for the coolest RGB stars, warmer RGB stars, and hot stars, all at 47 Tuc's metallicity. Lines that should appear in the Solar spectrum were also included. As shown below, the atomic data from VALD are not capable of reproducing the strengths or profiles of all the lines in

the Solar and Arcturus spectra. Thus, atomic data (i.e. $\log gf$ values, damping parameters, and wavelengths) were checked in both the Kurucz¹² and National Institute of Standards and Technology (NIST)¹³ databases. These atomic data were then adjusted so that the Solar and Arcturus spectra were accurately reproduced in the syntheses. The Final Line List also contains molecular lines from the Kurucz database, as described in Section 3.2.2.

3.2.1 Hyperfine Structure

Hyperfine structure (HFS) occasionally affects lines in the synthesized spectral regions. The HFS components are not included at this time (except for the case of the Eu II line in Section 4.3) though their presence is noted. All regions with possible HFS components were ignored when determining continuum levels. In the future these components can also be incorporated into the syntheses.

3.2.2 Molecular Lines

As discussed above, spectral lines from several important molecules (e.g., CH, CN, and MgH) are also included in the Final List when the lines were detected in the Arcturus Atlas (Hinkle

¹¹ <http://www.astro.uu.se/~vald/php/vald.php>

¹² <http://kurucz.harvard.edu/linelists.html>

¹³ <http://www.nist.gov/index.html>

Table 6. NGC 7006's CMD Boxes

	$V_{0,\text{avg}}$	$(V - I)_{0,\text{avg}}$	T_{eff} (K)	$\log g$	ξ (km/s)	R (R_{\odot})	$f(V)$	N
RGB	15.694	1.539	4022.	0.371	1.87	96.61	0.0197	1
	15.800	1.504	4058.	0.445	1.85	88.69	0.0357	2
	15.941	1.300	4333.	0.726	1.79	64.21	0.0157	1
	16.215	1.327	4271.	0.793	1.78	59.40	0.0122	1
	16.455	1.247	4389.	0.975	1.74	48.20	0.0195	2
	16.645	1.196	4469.	1.107	1.71	41.40	0.0327	4
	16.855	1.194	4465.	1.188	1.69	37.69	0.0472	7
	17.400	1.096	4644.	1.517	1.62	25.82	0.0568	14
	17.896	1.049	4735.	1.768	1.57	19.33	0.0460	18
	18.517	0.987	4738.	2.018	1.52	14.50	0.0895	62
19.211	0.930	4856.	2.357	1.44	9.81	0.0465	61	
20.276	0.876	4981.	2.845	1.34	5.59	0.0871	328	
SGB	21.312	0.808	5156.	3.339	1.23	3.17	0.0196	177
	21.607	0.663	5978.	3.765	1.14	1.94	0.0664	792
MS	22.181	0.627	6151.	4.048	1.08	1.40	0.0748	1516
	22.774	0.660	6022.	4.243	1.04	1.12	0.0491	1722
	23.392	0.722	5774.	4.409	1.01	0.92	0.0237	1467
	23.998	0.812	5439.	4.530	0.98	0.80	0.0070	759
	24.733	0.955	4804.	4.534	0.98	0.80	0.0021	454
AGB	16.429	1.101	4668.	1.141	1.70	39.81	0.0299	3
	17.233	1.008	4697.	1.481	1.63	26.91	0.0281	6
	17.694	0.941	4833.	1.739	1.57	19.99	0.0372	12
HB	18.496	0.823	5115.	2.197	1.48	11.81	0.0265	18
	18.718	0.663	5612.	2.489	1.42	8.43	0.0266	22
	18.747	0.493	6542.	2.809	1.35	5.83	0.0244	21
	18.638	0.244	7564.	3.040	1.30	4.47	0.0363	28
	18.713	0.093	8451.	3.240	1.26	3.55	0.0308	26
BS	21.184	0.407	7063.	3.912	1.11	1.63	0.0039	33
	20.583	0.209	7923.	3.883	1.12	1.69	0.0053	26

The 50% light level is $V_{1/2} = 18.75$, i.e. in the middle of the HB.

2003). The MOOG 1997 default values for the molecular equilibrium calculations were employed, with the exception of the MgH dissociation energy, for which the MOOG 2010 value was adopted.

Syntheses of these molecular features require input C and N abundances, and $^{12}\text{C}/^{13}\text{C}$ and $^{24}\text{Mg}:^{25}\text{Mg}:^{26}\text{Mg}$ ratios. For each cluster, “integrated” C and N abundances are derived to best fit the molecular lines—each integrated abundance is adopted for the whole cluster, and star-to-star variations are not considered. The observed isotopic ratios from individual stars can vary significantly, even within a single cluster. The $^{12}\text{C}/^{13}\text{C}$ ratio has been observed to vary from > 50 down to ~ 4 (Lambert & Ries 1981; Gilroy & Brown 1991; Gratton et al. 2000). In M 13, NGC 6752, and M 71, Yong et al. (2003, 2006) found $^{24}\text{Mg}:^{25}\text{Mg}:^{26}\text{Mg}$ ratios ranging from 48 : 13 : 39 to 83 : 10 : 7. Figure 5 shows the effects of varying the isotopic ratios, as well as the effects of neglecting all molecular lines, in the regions around the 5528 Å Mg I and the 6645 Å Eu II line (the regions with molecular lines, according to the Arcturus Atlas). Here $^{12}\text{C}/^{13}\text{C}$ ratios of 4, 9, and 50 are considered, as well as $^{24}\text{Mg}:^{25}\text{Mg}:^{26}\text{Mg}$ ratios of 48 : 13 : 39 and 83 : 10 : 7. In these regions, the isotopic ratios do not significantly affect the continuum levels, or the specific lines that are being synthesized. Hence, different isotopic ratios are not investigated in the ILS syntheses.

It should also be noted that none of the molecular lines have been calibrated to the Solar and Arcturus spectra (i.e. none of the atomic data, etc. were changed from the Kurucz values). Any regions with mismatching/uncertain molecular features (whether

from isotopic ratios or atomic data) are identified in the syntheses with the Final Line List.

3.2.3 Damping

Damping (e.g., from pressure broadening) can affect the abundances derived from strong lines. For consistency, damping is included for the strongest lines (in the Arcturus spectrum). The damping is implemented in ILABUNDS in a similar way as the 2010 version of MOOG, i.e. the damping parameters from Barklem et al. (2000) and Barklem & Aspelund-Johansson (2005) were converted to C6 parameters. When damping data were not available from the Barklem sources (or when they did not provide satisfactory fits to the Solar/Arcturus spectra), values from the VALD or Kurucz databases were included.

4 SPECTRUM SYNTHESIS RESULTS

Any rigorous spectrum synthesis method should yield abundances with random errors that are less than or equal to the standard error from an equivalent width analysis, whether for individual stars or an ILS (though an equivalent width analysis may still be the preferable choice when the line profiles are uncertain, or if the S/N is quite low). An equivalent width analysis of Fe I lines from a $R \approx 30,000$ and S/N ~ 100 spectrum of an RGB star results in a line to line scatter of $\sim \pm 0.1$ dex (e.g., Sakari et al. 2011). Since

Table 7. M15's CMD Boxes

	$V_{0,\text{avg}}$	$(V - I)_{0,\text{avg}}$	T_{eff} (K)	$\log g$	ξ (km/s)	R (R_{\odot})	$f(V)$	N	
RGB	12.452	1.361	4349.	0.446	1.85	88.58	0.0107	1	
	12.599	1.271	4464.	0.594	1.82	74.73	0.0373	4	
	12.830	1.228	4513.	0.724	1.79	64.33	0.0151	2	
	13.061	1.157	4617.	0.884	1.76	53.51	0.0967	16	
	13.569	1.082	4735.	1.160	1.70	38.93	0.0532	14	
	14.008	1.018	4710.	1.323	1.66	32.29	0.0532	21	
	14.484	0.967	4805.	1.566	1.61	24.41	0.0278	17	
	14.941	0.921	4898.	1.796	1.56	18.73	0.0706	66	
	15.503	0.880	4987.	2.064	1.51	13.75	0.0487	77	
	16.136	0.843	5073.	2.356	1.44	9.83	0.0383	108	
	16.814	0.800	5180.	2.673	1.38	6.82	0.0518	274	
	17.448	0.766	5270.	2.963	1.31	4.88	0.0342	323	
	SGB	18.069	0.702	5460.	3.285	1.25	3.37	0.0344	576
		18.366	0.556	5985.	3.588	1.18	2.38	0.0427	939
	MS	18.947	0.520	6612.	4.009	1.09	1.46	0.0863	3261
		19.649	0.554	6495.	4.252	1.04	1.11	0.0621	4473
		20.399	0.633	6164.	4.451	1.00	0.88	0.0414	5994
21.285		0.770	5617.	4.627	0.96	0.72	0.0183	6062	
22.352		0.971	4797.	4.715	0.94	0.65	0.0021	1886	
AGB/HB	12.923	1.100	4721.	0.892	1.75	53.02	0.0069	1	
	13.840	0.962	4814.	1.312	1.67	32.69	0.0260	9	
	14.632	0.864	5022.	1.733	1.58	20.14	0.0171	12	
	15.168	0.740	5345.	2.087	1.50	13.39	0.0171	20	
	15.570	0.562	5959.	2.474	1.42	8.58	0.0071	12	
	15.490	0.414	6832.	2.716	1.37	6.49	0.0084	13	
	15.399	0.244	7537.	2.864	1.34	5.47	0.0174	25	
	15.520	0.147	8051.	3.021	1.30	4.57	0.0383	61	
	15.637	0.052	8853.	3.195	1.26	3.74	0.0090	16	
	15.966	-0.032	10589.	3.491	1.20	2.66	0.0101	28	
	16.613	-0.111	13883.	3.958	1.10	1.55	0.0073	33	
	16.661	-0.199	19831.	4.232	1.04	1.13	0.0016	8	
	18.304	-0.273	23306.	4.983	0.88	0.48	0.0003	7	
BS	16.809	0.143	8198.	3.557	1.19	2.47	0.0038	21	
	18.375	0.228	7923.	4.115	1.07	1.30	0.0046	110	

The 50% light level for M15 is $V_{1/2} = 15.84$, which runs through the red HB stars.

Table 8. The Fe Line List.^a

Wavelength (Å)	Element	E.P. (eV)	$\log gf$	Equivalent width (mÅ)						
				Sun	Arcturus	47 Tuc	M3	M13	NGC 7006	M15
5324.191	Fe I	3.211	-0.103	-	-	-	112.0	97.2	103.0	38.6
5339.937	Fe I	3.266	-0.72	176.0	-	-	80.1	75.1	87.0	-
5367.476	Fe I	4.415	0.443	177.0	142.3	114.0	70.0	68.0	78.0	22.9
5369.974	Fe I	4.371	0.536	-	144.0	147.0	72.5	73.2	75.1	-
5371.501	Fe I	0.958	-1.644	-	-	-	183.0	167.6	186.0	108.6

Equivalent widths were measured in DAOSPEC; all strong lines were checked and refined in *splot*. The lines that were not measured in the Solar spectrum were those stronger than $EW > 150$ mÅ.

^aTable 8 is published in its entirety in the electronic edition of *MNRAS*. A portion is shown here for guidance regarding its form and content.

there are many Fe I lines, and each line is considered to be an independent measurement, the average Fe I abundance has a *random* error of $\sim 0.1/\sqrt{N}$ dex (though systematic uncertainties may be larger, as discussed by McWilliam et al. 1995a). However, for a single line, this random measurement error in the elemental abundance cannot be determined directly. Therefore ± 0.1 dex is adopted as the minimum uncertainty in the abundance of any single spectral line in an $R = 30,000$ and $S/N = 100$ spectrum. Since the GC ILS have these same qualities, the goal of this analysis is to reduce the spectrum synthesis abundance uncertainties to this minimum.

Sections 4.1, 4.2, and 4.3 show the integrated light syntheses of Mg, Na, and Eu lines in the ILS of the five Galactic GCs. Each section begins with syntheses of the 47 Tuc ILS, using the three different line lists (see Section 3.2). For each case, the errors due to continuum placement and profile fitting are discussed in detail, and it is shown that neither the Minimal nor VALD Line Lists are sufficient for reducing the errors to a satisfactory level. Each section then presents syntheses on the other Galactic GCs, using only the Final Line List.

Table 9. Fe Abundances.

	Arcturus		47 Tuc		M3		M13		NGC 7006		M15	
	[Fe/H]	<i>N</i>	[Fe/H]	<i>N</i>	[Fe/H]	<i>N</i>	[Fe/H]	<i>N</i>	[Fe/H]	<i>N</i>	[Fe/H]	<i>N</i>
[Fe I/H]	-0.65 ± 0.02	91	-0.81 ± 0.02	68	-1.48 ± 0.03	100	-1.53 ± 0.02	72	-1.46 ± 0.03	76	-2.30 ± 0.03	32
[Fe II/H]	-0.60 ± 0.04	5	-0.69 ± 0.04	4	-1.59 ± 0.03	5	-1.56 ± 0.02	3	-1.57 ± 0.03	6	-2.38 ± 0.10	1
<i>MB08</i> [Fe I/H]	-		-0.75 ± 0.03		-		-		-		-	
<i>MB08</i> [Fe II/H]	-		-0.72 ± 0.06		-		-		-		-	
<i>Literature</i> [Fe/H]	-0.58 ± 0.03		-0.72		-1.50		-1.53		-1.52		-2.37	

References: Literature values are from Yong et al. (2005) and Harris (1996; 2010 edition) for Arcturus and the target GCs, respectively. The MB08 values for 47 Tuc are also shown.

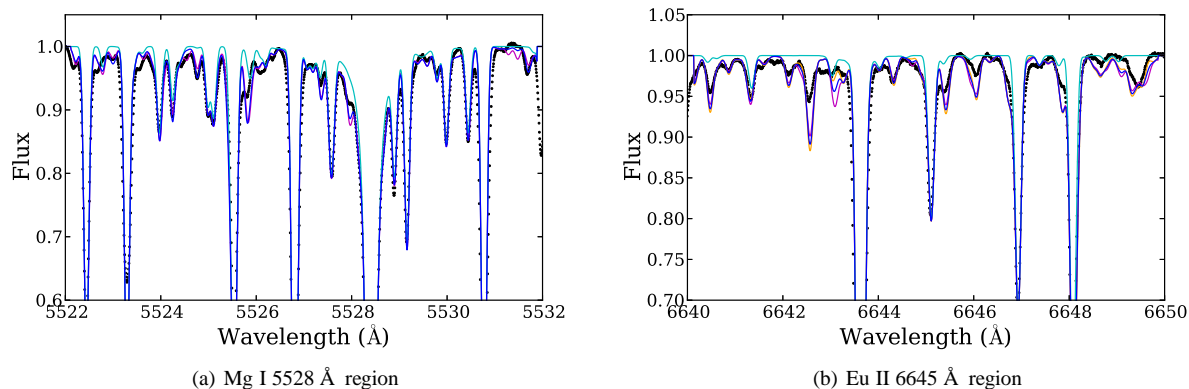


Figure 5. Syntheses of the Arcturus spectral regions around the 5528 Å Mg I (left) and 6645 Å Eu II (right) lines. The cyan lines show syntheses of only atomic lines (i.e. no molecular lines were included), with isotopic and HFS components included for the Eu II line in Figure 5b. It is evident that atomic lines do not account for all the lines in the regions. The Mg I region contains mainly MgH lines, while the Eu II region contains CN lines. The blue lines in the lefthand image indicate Mg isotopic ratios of 48 : 13 : 39 for ^{24}Mg : ^{25}Mg : ^{26}Mg (Yong et al. 2006), while the magenta lines indicate Mg isotopic ratios of 83 : 10 : 7 (Yong et al. 2003). The orange, blue, and magenta lines in the righthand image show $^{12}\text{C}/^{13}\text{C}$ ratios of 50, 9, and 4, respectively.

4.1 Mg I: The 5528 and 5711 Å lines

Magnesium is an important element in any abundance analysis. As an α -element, Mg can trace the chemical contributions from massive stars, particularly Type II supernovae. Additionally, its nucleosynthetic history is simpler than many other elements that form entirely through core burning in massive stars. In GCs, however, Mg has been observed to vary among stars in a single cluster (e.g. Shetrone 1996; Gratton et al. 2004), which means that an ILS abundance may not reflect the “primordial” α -abundance of the cluster. The effects of star-to-star chemical variations will be investigated more in the future—the current work is limited to a single ILS Mg abundance per cluster.

4.1.1 Mg in 47 Tuc: The Minimal and VALD Line Lists

This section first presents spectrum syntheses of the 47 Tuc ILS Mg I lines using only the lines in the Minimal and VALD Line Lists. This is to show that a complete line list that has been calibrated to the Sun and Arcturus is necessary, and affects the precision of the results. The next section (Section 4.1.2) presents results with the best Final Line List.

4.1.1.1 5528 Å The 5528 Å feature is typically strong in metal-rich ([Fe/H] $\gtrsim -1.0$) stars. In the 47 Tuc spectrum, the equivalent width of this line is ~ 230 mÅ, making the line too strong for an abundance analysis, since the uncertainties in damping, stellar

structure, and NLTE corrections become too large. However, this 5528 Å feature is not as strong in the more metal-poor clusters (such as M3, M13, NGC 7006, and M15), and the spectral region must therefore be calibrated.

Figure 6 shows syntheses of the 5528 Å line in 47 Tuc with the two basic line lists. The top panel shows the syntheses with lines only from the Minimal List, while the middle panel shows the syntheses with the VALD Line List. In addition to the Mg I line, only two other lines are in the Minimal List (an Fe I line at 5522.45 Å, and a Sc II line at 5526.82 Å). The scarcity of lines makes it very difficult to distinguish weak lines from noise. This leads to large uncertainties in continuum placement, as shown by the large vertical offsets. This uncertainty leads to Mg abundance errors that are ~ 0.20 dex, which is insufficient for distinguishing between a Mg-enhanced and non-Mg-enhanced cluster.

The VALD line list (which includes more lines) helps significantly with continuum identification. Different continuum shifts are still necessary in order to fit the different features, and it is still difficult to distinguish weak features from noise. In this case, the best-fitting synthesis leads to Mg abundance errors that are ± 0.15 dex—this uncertainty is lower than before, but is still large.

4.1.1.2 5711 Å The only RGB line from the Minimal List that appears in this spectral region is the 5711 Å Mg I line itself. Without any additional lines in the region, it is difficult to locate the continuum level in the region, as illustrated by the synthesis of 47 Tuc

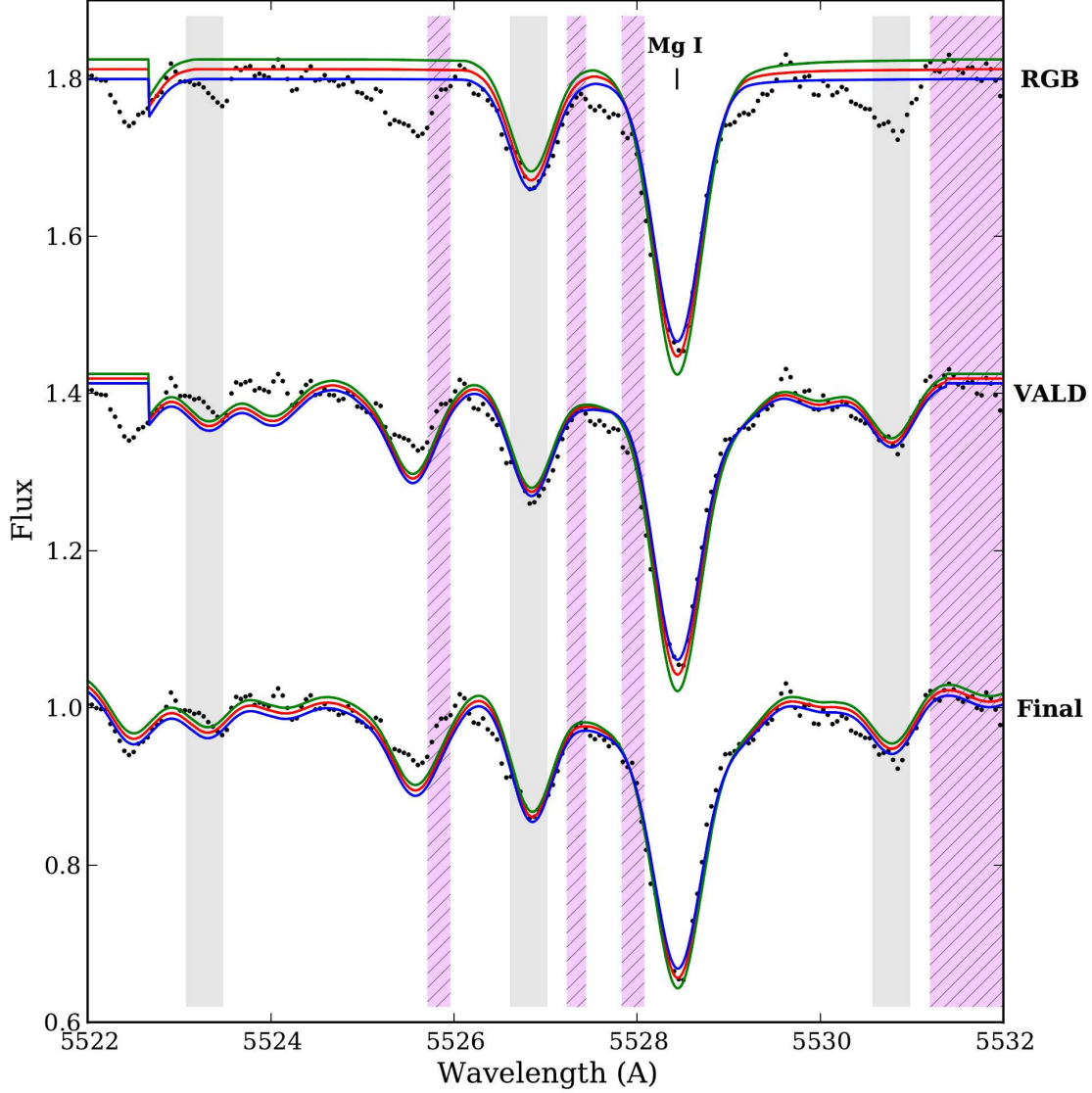


Figure 6. Spectrum syntheses of the 5528 Å Mg I line on the 47 Tuc ILS with the Minimal, VALD, and Final Line Lists. Uncertainties in continuum location and line profile fitting are both considered. The red lines show the average abundance, while the green/blue lines show the $\pm 1\sigma$ abundances, respectively. The shaded grey regions indicate areas with possible HFS components, while the hatched light purple regions indicate uncertain molecular features. Both types of regions have been ignored for continuum fits.

in Figure 7. In particular, it is unclear whether the peak blueward of the 5711 Å line is the true continuum, noise, an improperly removed cosmic ray, etc. It is also unclear whether the width or depth of the line should be fit. Considering all these factors, the uncertainty in the best-fitting abundance ends up being ± 0.25 .

As before, the increased number of lines in the VALD Line List helps to isolate the continuum level. However, many of the synthesized lines in the region do not match the observed ones—some are stronger, others are weaker, and some are missing altogether. With the VALD lines, the error in the best fitting abundance becomes ± 0.17 . This level of uncertainty is better, but is still less

than expected for a spectrum synthesis on such a high S/N spectrum (~ 100).

Thus, the Minimal and VALD line lists are insufficient for the ILS syntheses of the regions around these two Mg I lines, primarily because the continuum level cannot be clearly identified. These lists may be missing spectral lines (which are blended together in the ILS)—furthermore, the lines that *are* in the lists do not all fit the observed lines properly. This suggests that the line lists must be tested and *calibrated* on well-studied stars, such as the Sun and Arcturus.

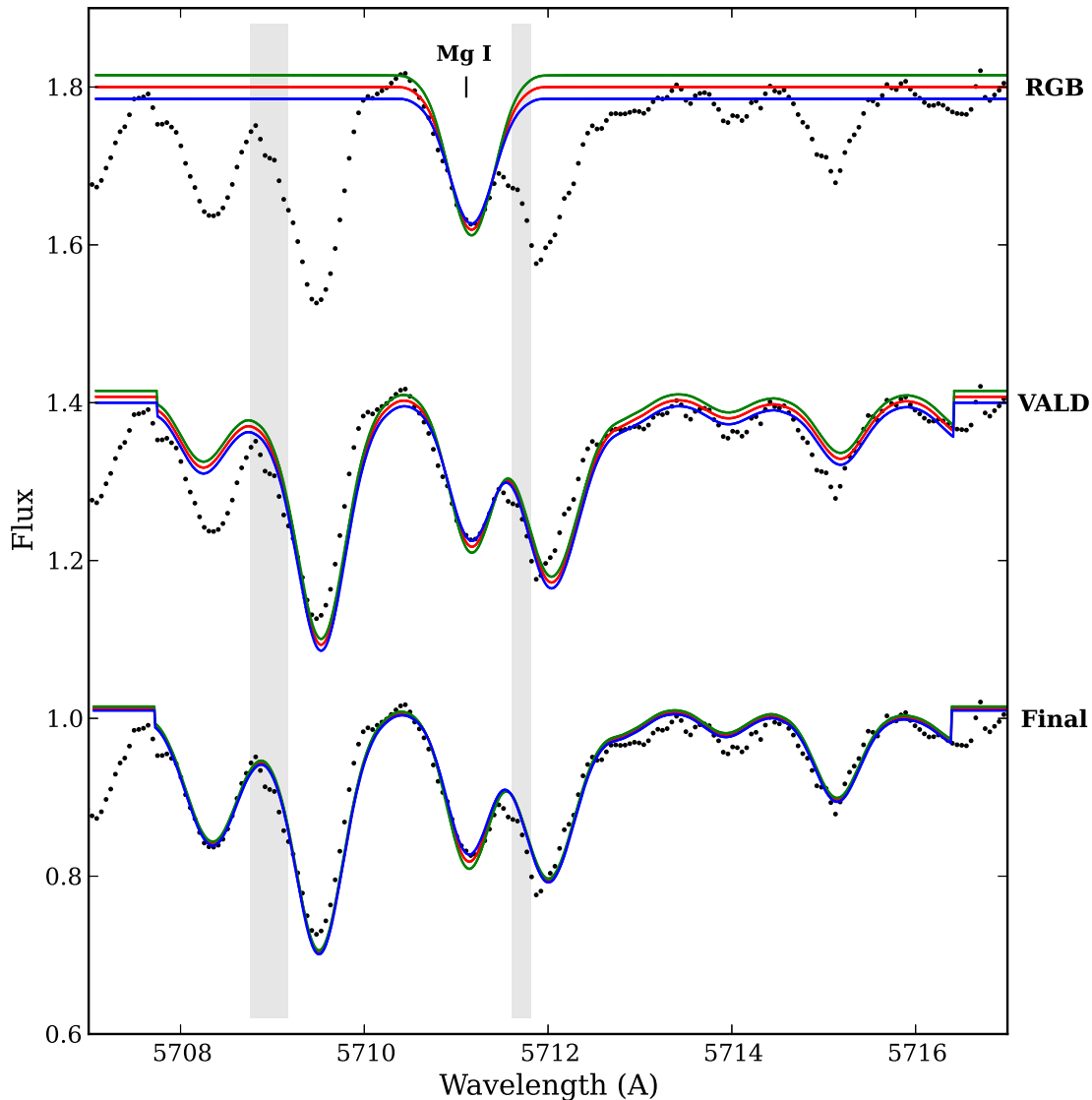


Figure 7. Spectrum syntheses of the 5711 Å Mg I line on the 47 Tuc ILS with the Minimal, VALD, and Final Line Lists. Lines are as in Figure 6.

4.1.2 Mg in 47 Tuc: The Final Line List

This section presents syntheses of the Mg I lines in the Solar, Arcturus, and 47 Tuc spectra with the complete, calibrated Final Line Lists. The regions with possible HFS components are highlighted in purple, while the regions with particularly uncertain molecular lines are highlighted with grey, hatched rectangles. These regions (and any with missing lines) were ignored in the final synthesis fits.

4.1.2.1 5528 Å The syntheses to the 5528 Å line are shown in Figures 6 and 8, while the final abundances are tabulated in Table 10. The addition of the MgH features in the Final Line List helps improve the continuum identification, particularly for the blended features in 47 Tuc. Despite the strength of the line, the synthesis of

the 5528 Å feature fits the Solar spectrum quite well (see the top panel of Figure 8). The best-fitting value is slightly higher than the Asplund et al. (2009) value, but is likely due to the strength of the line and the uncertain atomic data. The Arcturus abundance agrees well with the average literature value in Table 10.

In the 47 Tuc spectrum, the complete, calibrated line list leads to a synthetic spectrum that is an excellent fit to the observed spectrum, as shown in Figure 8. This is due to two reasons: first, most of the lines in the region now fit better than before they were calibrated, and second, the best continuum regions are evident in the Solar and Arcturus spectra, and can be used to fit the 47 Tuc continuum. However, the 47 Tuc syntheses indicate a best-fitting [Mg/Fe] ratio that is higher than the MB08 value of $[Mg/Fe] = 0.22$

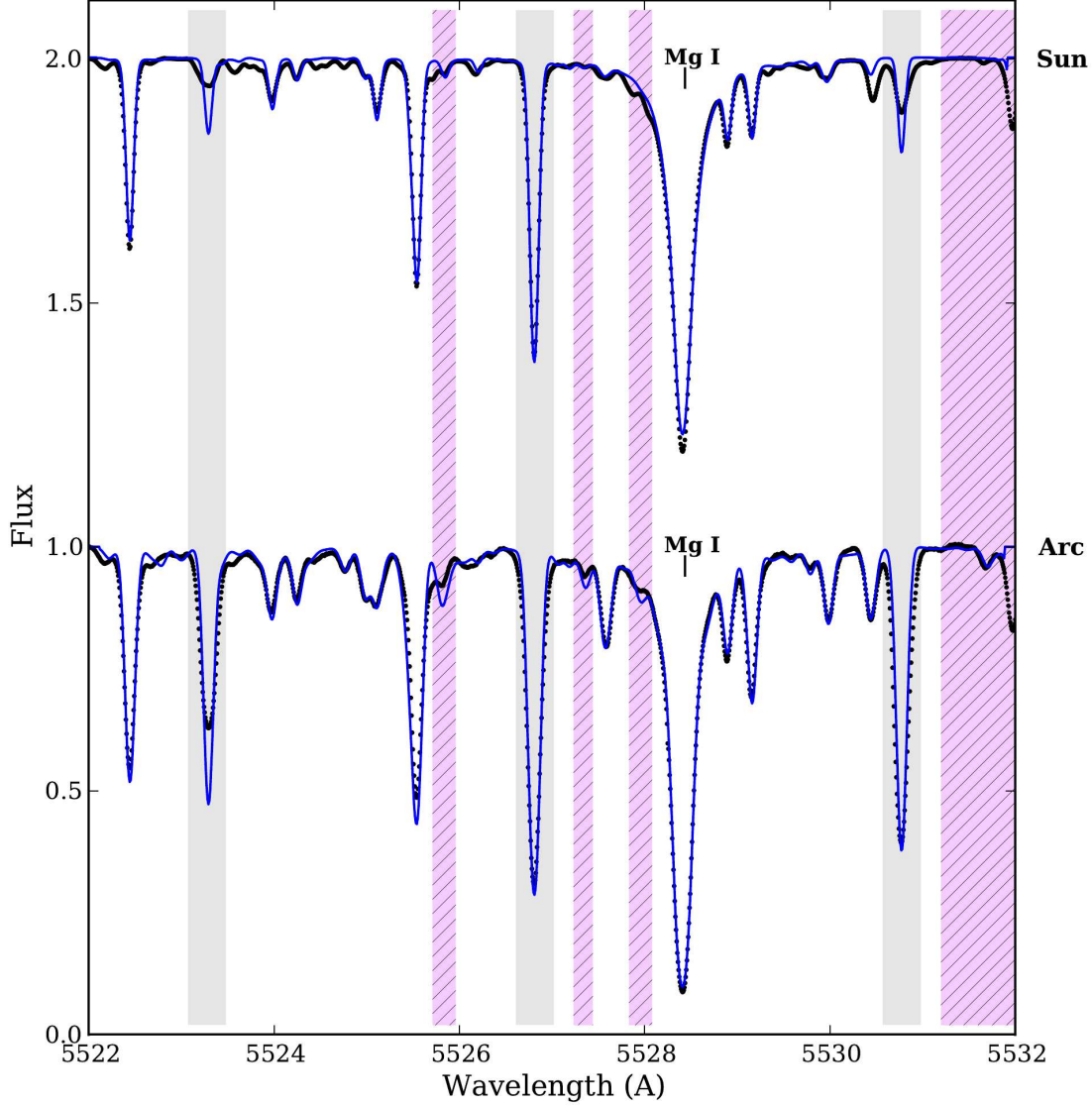


Figure 8. Spectrum syntheses of the 5528 Å Mg I line in the Solar (top) and Arcturus (bottom) spectra. Lines are as in Figure 6. Note that only the best fits are shown, as the differences in the $\pm 1\sigma$ syntheses are generally too small to see.

(which was determined from the EW of the 7387 Å Mg I line, and which was not calculated differentially). Adjusting the MB08 Solar abundance leads to a higher [Mg/Fe] ratio in 47 Tuc, as shown below.

4.1.2.2 5711 Å The syntheses of the 5711 Å Mg I line are shown in Figures 7 and 9. These fits show that there are missing lines in the syntheses of this region of the Solar and Arcturus spectra, even with a complete, calibrated line list. Several lines in the region also require HFS components, e.g. the V I and Sc I lines. Despite the missing features, the strong lines are generally matched well in both the individual and 47 Tuc spectra, with the exception of the feature at 5709 Å. This feature is a blend of Ti I, Fe I, Ni I,

and Ti II features, where the Fe I and Ni II features dominate the line strength. It is unclear why the lines match in the Solar spectrum, but not in the Arcturus or 47 Tuc spectra. Regardless, these features can be disregarded in the analyses.

The derived abundances are again tabulated in Table 10, along with comparison literature abundances. The Solar abundance is in excellent agreement with the Asplund et al. (2009) value. The Arcturus [Mg/Fe] ratio is slightly higher than the average literature value, but the values agree within the errors. The 47 Tuc [Mg/Fe] ratio is again considerably higher than the MB08 value ([Mg/Fe] = 0.22), but is in excellent agreement with the values from the 5528 Å line and with the recalculated MB08 value (see below).

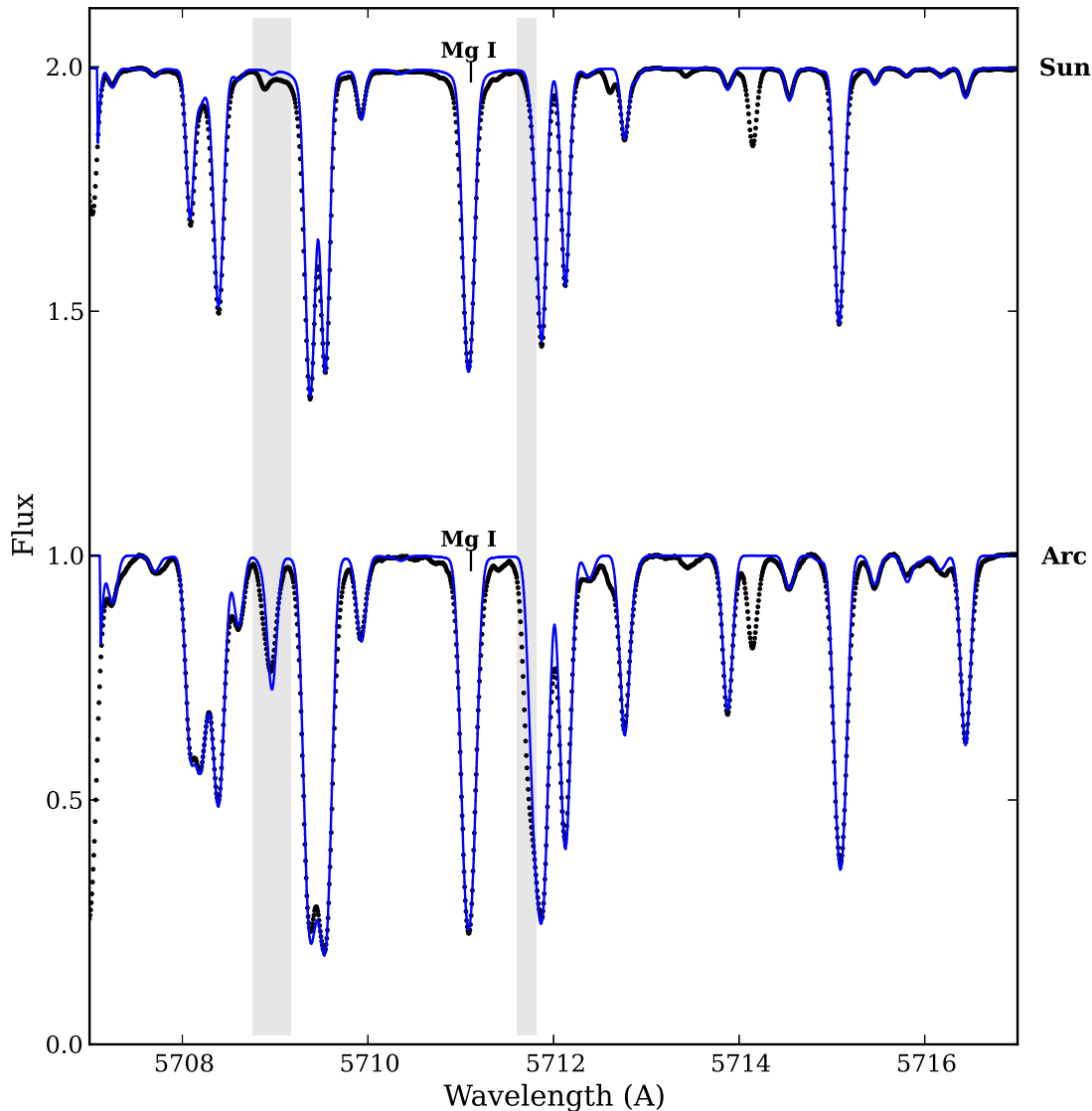


Figure 9. Spectrum syntheses of the 5711 Å Mg I line in the Sun and Arcturus. Lines are as in Figure 8.

Taken together, the two Mg I lines provide a total $[\text{Mg I}/\text{Fe I}] = 0.46 \pm 0.14$ for 47 Tuc. This *qualitatively* agrees with the literature stellar abundances assembled by Pritzl et al. (2005), i.e. 47 Tuc is Mg-enhanced, as expected for a Galactic GC at its metallicity, and the ILS value is in good agreement with the literature average. Ultimately, the calibrated Final Line List has reduced uncertainties in the Mg abundance ratios from the Minimal and VALD Lists from ~ 0.2 and ~ 0.18 to ~ 0.14 . Thus, spectrum synthesis techniques with the carefully calibrated Final Line List are able to provide improved and precise abundances.

4.1.2.3 7387 Å To compare the above Mg I integrated light abundances with MB08, the 7387 Å line was synthesized in the

Solar, Arcturus, and 47 Tuc spectra using the VALD RGB Line List only (Figure 10). This region was not calibrated because it falls outside the observed spectral region of the HET clusters, and will not be used in this analysis. Many of the lines in the region do not fit well, precisely because they have not been calibrated. Molecular lines and HFS components were also not included, although the Arcturus Atlas (Hinkle 2003) shows that there are CN lines in the region.

The Solar synthesis in Figure 10 shows that a Solar abundance of $\log \epsilon_{\text{Mg}} = 7.30 \pm 0.02$ is required to fit the observed feature; this value is significantly lower than the Asplund et al. (2009) Mg abundance. The line profile also cannot be fit perfectly, as there seem to be extra components in the red wing of the Mg I

line. The Arcturus synthesis fit is better, but the Mg abundance ($\log \epsilon_{\text{Mg}} = 7.15 \pm 0.03$) is lower than from the other Mg lines; a differential comparison with the lower Solar abundance leads to a normal $[\text{Mg I}/\text{Fe I}] = 0.50 \pm 0.04$. This suggests that the atomic data is systematically offset for this line, and illustrates the importance of using differential abundances and of checking all important lines in the Solar and Arcturus spectra.

Syntheses of the 47 Tuc ILS yield $\log \epsilon_{\text{Mg}} = 7.21 \pm 0.20$, or $[\text{Mg I}/\text{Fe I}] = 0.72 \pm 0.20$. The large uncertainty in the abundance reflects the uncertainty in the continuum level, the uncertain line profile, and the low S/N at the line center. With the Solar Mg abundance from the 7387 Å line, the MB08 value (which comes from an EW analysis of this line) can be recalculated *differentially* to $[\text{Mg I}/\text{Fe I}] = 0.56$ —this value now agrees with the 7388 Å, 5528 Å, and 5711 Å syntheses. Thus, the value quoted in MB08 is systematically lower than it should be, as a result of the lower Solar abundance.

4.1.3 Mg in the Other GCs

The Mg I abundances for M3, M13, NGC 7006, and M15, as determined from the Final Line List, are shown in Table 10 and Figures 11 and 12.

The fits to the Mg I lines are quite good for M3 and M13, but are much more uncertain for NGC 7006 (owing to its lower S/N) and M15 (as a result of its weaker lines). The 5528 Å line is easily detectable in all spectra, and there are enough additional lines to help isolate the continuum. The 5711 Å region, however, is much more difficult for M15, as is evident in Figure 12; this line only provides an upper limit for the Mg abundance in M15. The final derived abundances are shown in Table 10.

The average Mg I ILS abundance ratios for M3, M13, and NGC 7006 are in excellent agreement with each other. With the exception of M13, all the ILS values are slightly lower than the average literature abundances, especially M15. These differences between the ILS abundances and the “average” literature abundances are due to the known star-to-star Mg variations within the clusters. For example, the M15 Mg abundance quote in Pritzl et al. (2005) is an average of eighteen bright RGB stars observed by Sneden et al. (1997); the latter analysis showed that M15 has strong star-to-star Mg variations, ranging from $-0.4 \lesssim [\text{Mg}/\text{Fe}] \lesssim +0.8$, with $[\text{Mg}/\text{Fe}]$ decreasing for stars higher up the RGB. Since ILS are dominated by the brightest stars, the M15 ILS is most likely dominated by the most Mg-poor giants, which decreases the integrated light Mg abundance. The derived ILS $[\text{Mg}/\text{Fe}]$ ratio for M15 *does* fall at the lower end of the observed abundance range. M3 and M13 also show signs of Mg variations (Sneden et al. 2004; Cohen & Melendez 2005) which most likely accounts for their slightly low average $[\text{Mg}/\text{Fe}]$ abundances in comparison to Milky Way field stars. However, even though these clusters also have star-to-star variations, their abundances *do* agree with the literature averages. This shows that caution must be taken when comparing ILS abundances to “average” literature abundances from a limited sample of stars, as discussed in Section 5.2. Regardless, these comparisons with the literature abundances *do* show that spectrum syntheses of the 5528 and 5711 Å lines are capable of producing Galactic GC Mg I abundances that fall within the observed ranges from individual stars, provided that the lines are sufficiently strong, and that the S/N is sufficiently high.

4.2 Na I 6154/6160 Å lines

Sodium has always been an interesting element for GC studies because, like magnesium, it varies strongly between stars in a single cluster. These variations are anticorrelated with O, and indicate abundance changes up the RGB and/or the presence of multiple stellar populations in GCs (e.g. Kraft et al. 1992; Gratton et al. 2004; Carretta et al. 2009). The Na/O anticorrelation has been detected in all unambiguous Galactic GCs, and seems to be a common signature of the GC formation process. Thus, Na is another significant element in GC studies.

Sodium lines are known to suffer from strong non-LTE effects. To minimize NLTE effects, Lind et al. (2011) suggest that analyses at Solar metallicity should use the 6154/6160 Å doublet, while analyses of more metal-poor stars ($[\text{Fe}/\text{H}] \lesssim -1.0$) should use the 5682/5688 Å lines. However, literature results use both sets of lines, often without any NLTE corrections. Here the results for the 6154/6160 doublet are presented for all the GCs. The NLTE effects make it difficult to fit the Solar 5682/5688 Å lines (in agreement with, e.g., Baumüeller et al. 1998), which prevents a differential analysis from being done. Without a differential analysis the atomic data can lead to systematic offsets between lines. Further calibration work must therefore be done to synthesize the 5682/5688 Å doublet in ILS.

Mashonkina et al. (2000) also note that for all Na lines the strengths of NLTE corrections depend on the temperature and surface gravity of the stars, in addition to the stellar metallicity, and that Na abundances of giants cannot be accurately determined to within 0.1 dex without NLTE corrections. This could be particularly problematic for ILS, whose spectral lines contain contributions from stars over a wide range of T_{eff} and $\log g$. Despite these concerns, NLTE corrections are neglected in this analysis. However, as NLTE corrections are not generally applied to the comparison literature data, differential comparisons should be reasonably robust.

4.2.1 Na in 47 Tuc: The Minimal and VALD Line Lists

Figure 13 shows spectrum syntheses of the 6154/6160 Å doublet in 47 Tuc, using the Minimal and VALD Lists. The synthesis with the Minimal Line List (the top synthesis in Figure 13) only has a few strong lines available for continuum identification. Furthermore, the features are strongly blended in the 47 Tuc spectrum, and there are few obvious continuum locations. With only these strong lines, the errors in the best-fitting abundances are ± 0.30 and ± 0.13 for 6154 and 6160 Å, respectively. The VALD lines (the middle spectrum in Figure 13) help slightly, bringing the abundance errors to ± 0.25 and ± 0.12 , respectively.

With so many strong lines and blends in the region, it is easy to see how fitting becomes very difficult in ILS. In particular, it is difficult to isolate continuum regions and to know which regions *should* match the synthetic spectra, and which could be different as a result of improper atomic data, missing atomic or molecular lines, or HFS. Without Solar and Arcturus calibrations to identify the best areas for continuum fitting, such a region is quite difficult to fit in ILS.

4.2.2 Na in 47 Tuc: The Final Line List

Figures 13 and 14 show syntheses of the 6154 and 6160 Å Na I lines in the Solar, Arcturus, and 47 Tuc spectra with the Final Line List.

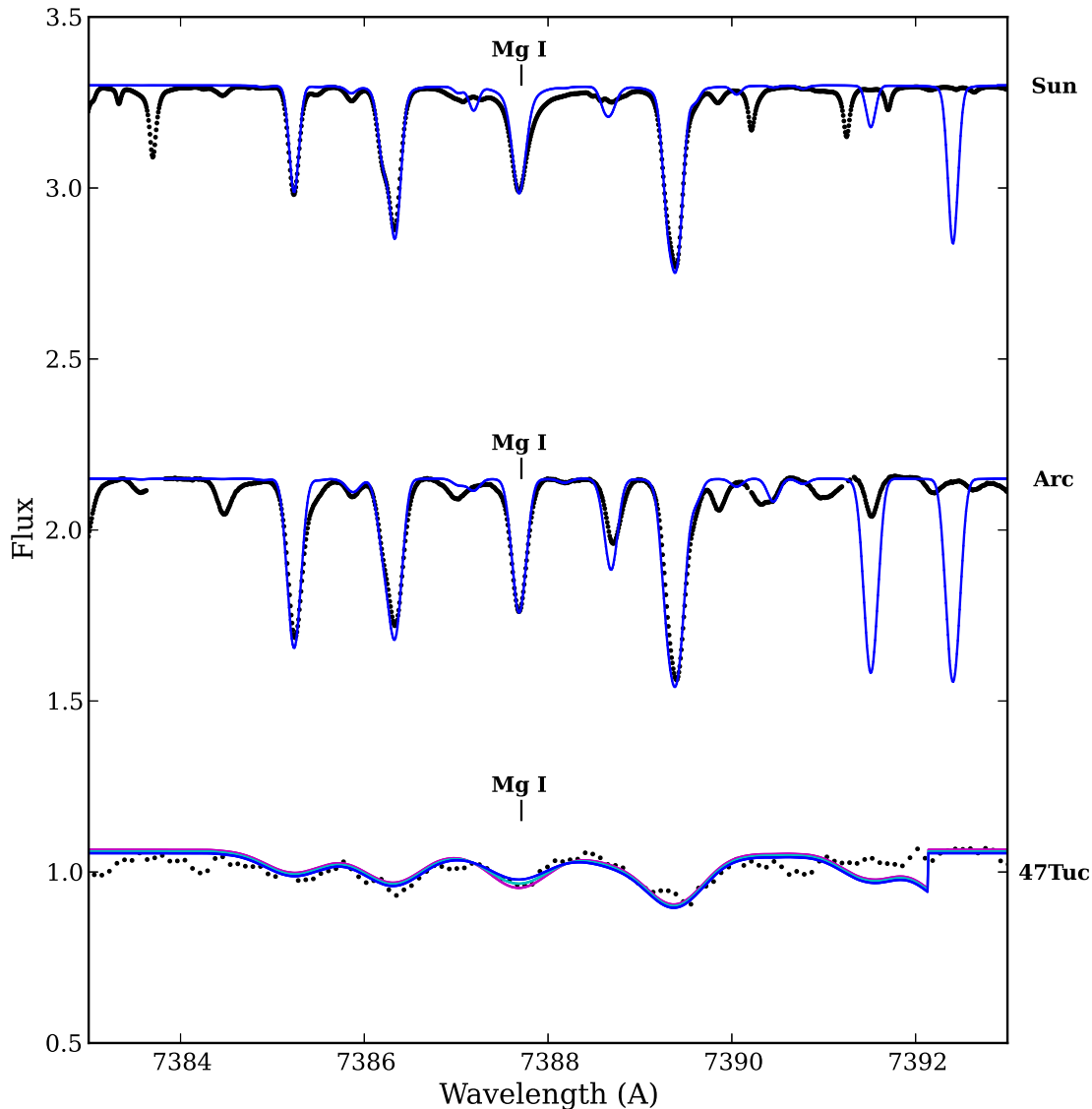


Figure 10. Spectrum syntheses of the 7388 Å Mg I line in the Solar (top), Arcturus (middle), and 47 Tuc (bottom) spectra. The HFS regions are not shown, though there are several in this wavelength range. Molecular lines are also not included. Lines are as in Figure 6.

HFS contamination seems to be minimal in this region. The Solar and Arcturus syntheses show that there are clearly lines missing from the line list, though they are mostly weak. The Solar and Arcturus spectra also show that the syntheses cannot perfectly reproduce the shape of the 6154 Å Na I line—there seems to be a missing component slightly redward of the line center. Thus, the syntheses to the 47 Tuc spectrum focused primarily on fitting the depth of the line rather than the width.

The best fit abundances to the 6154/6160 Å Na I lines are shown in Table 10. The Solar values are in reasonable agreement with the Asplund et al. (2009) value. The Arcturus value is also in excellent agreement with the average literature value, after shifting to a common [Fe/H]. The 47 Tuc value is in agreement with

the MB08 value, which was derived from the same lines. The integrated light abundance also agrees well with the average literature abundance in Table 10. As a Galactic GC, 47 Tuc is one of the many Galactic GCs that have shown star-to-star variations in Na, as mentioned earlier (e.g. Carretta et al. 2009). However, in this case the Na abundance is not overly high, suggesting that the integrated light is not dominated by Na-enhanced stars.

For the 6154 Å sodium line, the Final Line List has reduced the errors from 0.30 (from the Minimal Line List) and 0.25 (from the VALD Line List) to 0.15. In the case of the 6160 Å line the improvements are similarly excellent, with decreases from 0.13 and 0.13 to 0.07. Again, the Final Line List provides a significant improvement to the precision of the derived ILS abundances.

Table 10. Solar, Arcturus, and Globular Cluster Abundances

	Sun log ϵ_{\odot}	Arcturus [X/Fe]	47 Tuc [X/Fe]	M3 [X/Fe]	M13 [X/Fe]	NGC 7006 [X/Fe]	M15 [X/Fe]
Mg 5528 Å	7.75 ± 0.05	0.55 ± 0.18	0.39 ± 0.13	0.12 ± 0.11	0.13 ± 0.11	0.10 ± 0.14	-0.15 ± 0.21
Mg 5711 Å	7.58 ± 0.04	0.59 ± 0.06	0.44 ± 0.14	0.20 ± 0.07	0.14 ± 0.08	0.13 ± 0.20	< 0.55
Mg Total	—	0.57 ± 0.13	0.42 ± 0.14	0.16 ± 0.11	0.14 ± 0.10	0.12 ± 0.17	—
MB08			$0.22/0.56^a$				
Literature Avg	7.60 ± 0.04	0.46 ± 0.09^b	0.40 ± 0.03	0.23 ± 0.03	0.11 ± 0.03	0.34 ± 0.02	0.35 ± 0.05
Lit. Range	—	—	[0, +0.6]	[−0.1, +0.6]	[−0.2, +0.5]	[+0.3, +0.4]	[−0.4, +0.8]
Na 6154 Å	6.28 ± 0.02	0.20 ± 0.03	0.38 ± 0.15	0.27 ± 0.13	0.45 ± 0.10	0.66 ± 0.14	0.90 ± 0.40
Na 6160 Å	6.33 ± 0.03	0.20 ± 0.04	0.37 ± 0.08	0.17 ± 0.13	0.20 ± 0.20	0.26 ± 0.13	< 1.05
Na Total	—	0.20 ± 0.04	0.38 ± 0.12	0.22 ± 0.13	0.33 ± 0.16	0.41 ± 0.14	—
MB08			0.45 ± 0.10				
Literature Avg	6.24 ± 0.04	0.18 ± 0.05^b	0.45 ± 0.01	0.02 ± 0.06	0.27 ± 0.06	0.32 ± 0.06	0.39 ± 0.06
Lit. Range	—	—	[−0.3, +1.0]	[−0.3, +0.3]	[−0.3, +0.6]	[0, +0.4]	[−0.6, +2.0]
Eu 6645 Å	0.45 ± 0.02	0.28 ± 0.05	0.27 ± 0.14	0.75 ± 0.11	0.76 ± 0.10	0.72 ± 0.15	1.31 ± 0.20
MB08			0.04				
Literature Avg	0.52 ± 0.04	0.26 ± 0.04	0.14 ± 0.03	0.51 ± 0.02	0.49 ± 0.03	0.36 ± 0.02	0.63 ± 0.03
Lit. Range	—	—	[−0.4, +0.4]	[+0.4, +0.8]	[+0.3, +1.0]	[+0.3, +0.4]	[+0.2, +2.2]

The [X/Fe] ratios use Fe I for neutral species, and Fe II for singly ionized species. The mean literature values are straight, un-weighted averages from all available sources. The quoted $\pm 1\sigma$ errors in the literature mean do not reflect the observed range in the abundances. The literature ranges show the approximate extremes that have been observed in the clusters. Flux-weighted averages may be more appropriate for comparisons with integrated light abundances; however, these averages require a reasonably complete sample that reflects the scanned population.

References: Literature Solar values are from Asplund et al. (2009). Arcturus literature values are an average of the values from Yong et al. (2005), Fulbright et al. (2007), Ramírez & Allende Prieto (2011), and McWilliam et al. (2013, in prep; for Eu), after shifting to a common [Fe/H] = −0.6. The GC literature data are from observations of individual stars, and are from Pritzl et al. (2005), with supplements from Brown & Wallerstein (1992); Sneden et al. (1997); Kraft et al. (1998); Sneden et al. (2004); Carretta et al. (2004); Jasniewicz et al. (2004); Cohen & Melendez (2005); Alves-Brito et al. (2005); Preston et al. (2006); Wylie et al. (2006); Koch & McWilliam (2008); Carretta et al. (2009); Worley et al. (2009); Sobeck et al. (2011); Gratton et al. (2013). The 47 Tuc values from MB08 are also shown.

^aThe first value is the one quoted in MB08; the second is the re-derived *differential* value (see the text).

^bValues were adjusted to [Fe/H] = −0.6.

4.2.3 Na in the Other GCs

The Na 6154/6160 Å syntheses on M3, M13, NGC 7006, and M15 are shown in Figure 15, while the abundances are given in Table 10. The comparison literature abundances are also shown in Table 10. These literature abundances were determined with both the 6154/6160 and 5682/5688 Å lines (and occasionally also the Na D lines). In the case of M3, M13, and NGC 7006, the literature abundances have *not* had NLTE corrections, while some of the M15 stars did have NLTE corrections. The M3/M13 literature abundances are from 36 and 60 stars from the base of the RGB, up to the tip of the RGB, while the NGC 7006 literature abundances are only from six tip of the RGB stars. M15's literature abundances are mainly from more evolved stars (e.g. RGB, HB, and AGB stars).

While M13 and NGC 7006's ILS abundances are in good agreement with the literature averages, the IL Na abundance in M3 is quite a bit higher than the average literature value. The 6160 Å line is not well-resolved in the M15 ILS, and hence provides only an upper limit. The 6154 Å line in M15, however, provides a larger Na abundance than the literature average. Again, these discrepancies with the literature averages are results of the intercluster Na variations, which vary from $-0.6 \lesssim [\text{Na}/\text{Fe}] \lesssim 2$ (Sneden et al. 1997; Preston et al. 2006).

4.3 Eu II 6645 Å line

The weak 6645 Å Eu II feature is commonly synthesized in spectroscopic analyses, since it provides important constraints on contributions from the r- (rapid) neutron capture process.¹⁴

4.3.1 Eu in 47 Tuc: The Minimal and VALD Line Lists

The 47 Tuc syntheses with the Minimal and VALD Lists are shown in Figure 16. There appear to be fewer lines in this region, making it easier to identify the continuum level. Altogether, the errors in the abundances are ± 0.17 and ± 0.15 for the Minimal List and the VALD RGB List, respectively.

4.3.2 Eu in 47 Tuc: The Final Line List

With the Final Line List, syntheses of the Eu II line in the Solar, Arcturus, and 47 Tuc spectra are shown in Figures 16 and 18. HFS and isotopic components for the Eu II line are included, using the data from Lawler et al. (2001)—these corrections alter the shape of the line slightly, but have a negligible effect on its equivalent width. There are several other lines with HFS components in the region of the Eu II line which are not included.

¹⁴ At solar metallicity 97% of Eu comes from the r-process (Burris et al. 2000).

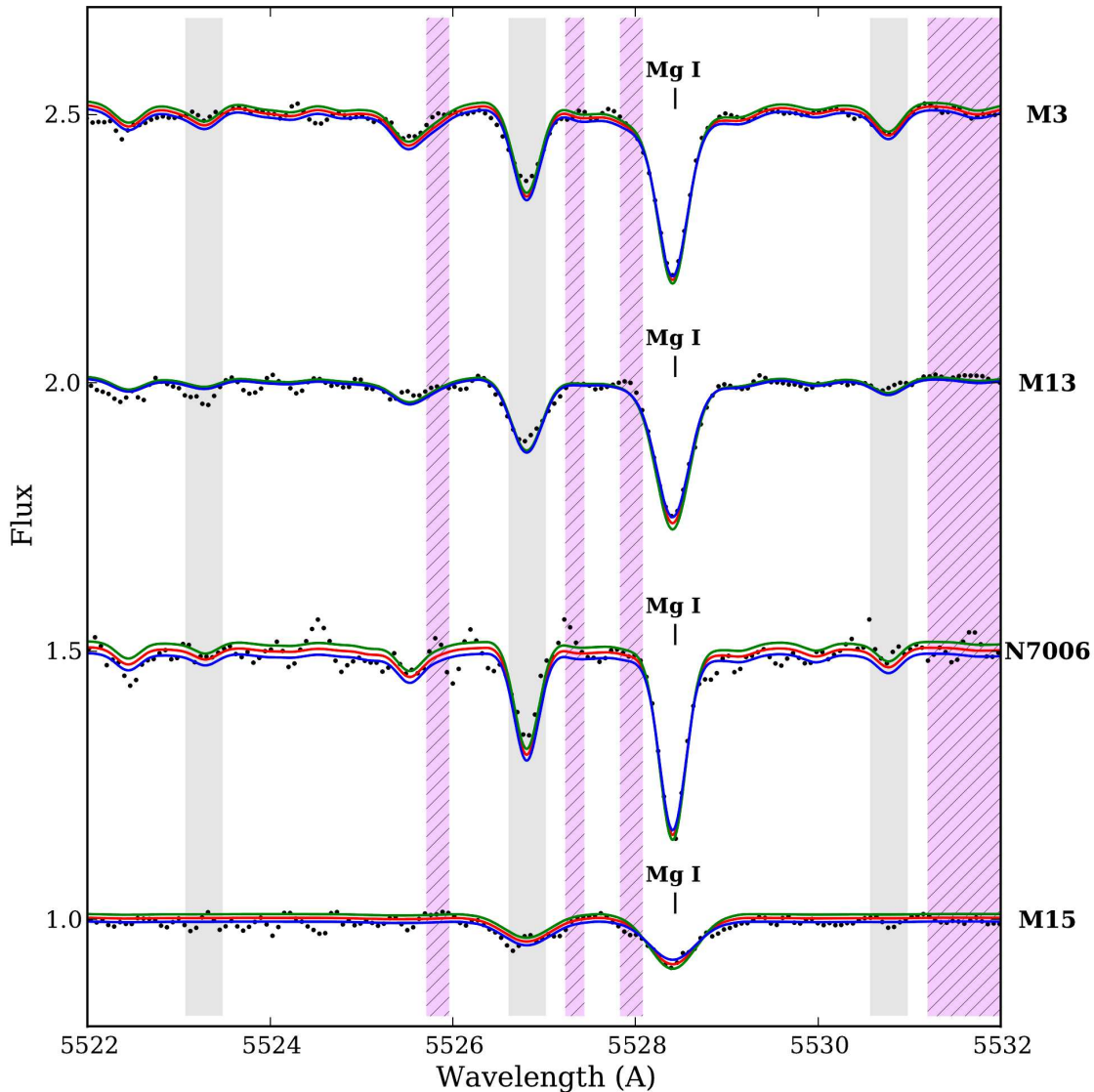


Figure 11. Spectrum syntheses of the 5528 Å Mg I line in M3, M13, NGC 7006, and M15. Lines are as in Figure 6.

As discussed earlier, CN molecular lines are present throughout the region around the 6645 Å Eu II line. For the Solar syntheses the C and N abundances from Asplund et al. (2009) are used, while scaled-Solar C and N abundances are adopted for Arcturus. For 47 Tuc it is less clear which C and N abundances to use. The effects of dredge-up in RGB stars (e.g. C depletion and N enhancement; Lambert & Ries 1981) are likely to influence the integrated light abundance. In addition, all the stars in 47 Tuc show a well-established CN bimodality, from the RGB (e.g. Briley 1997) down to the main sequence (e.g. Briley et al. 2004). To determine the extent to which the input C and N abundances affect the ILS results, spectrum syntheses were performed with the extreme values deter-

mined from individual stars, i.e. $[C/Fe] \approx -0.8$ and $[N/Fe] \approx 0.0$ vs. $[C/Fe] \approx +0.4$ and $[N/Fe] \approx +2.0$ (Briley et al. 2004).

The 47 Tuc spectrum syntheses with different carbon abundances are presented in Figure 17. All syntheses were vertically shifted to fit the continuum regions, and the Eu II abundances were re-derived to best fit the line profile. The differences in the strengths of the CN lines are quite striking—in general the CN-weak case (in blue, i.e. the higher carbon abundance) has stronger spectral lines than the CN-strong case (in cyan). The unfortunate presence of a blended CN line redward of the Eu II line makes the Eu abundance particularly sensitive to the input C abundance. In order to force the CN-weak syntheses to best match the observed line profile, a Eu II abundance that is ~ 0.2 dex lower than the CN-strong case must

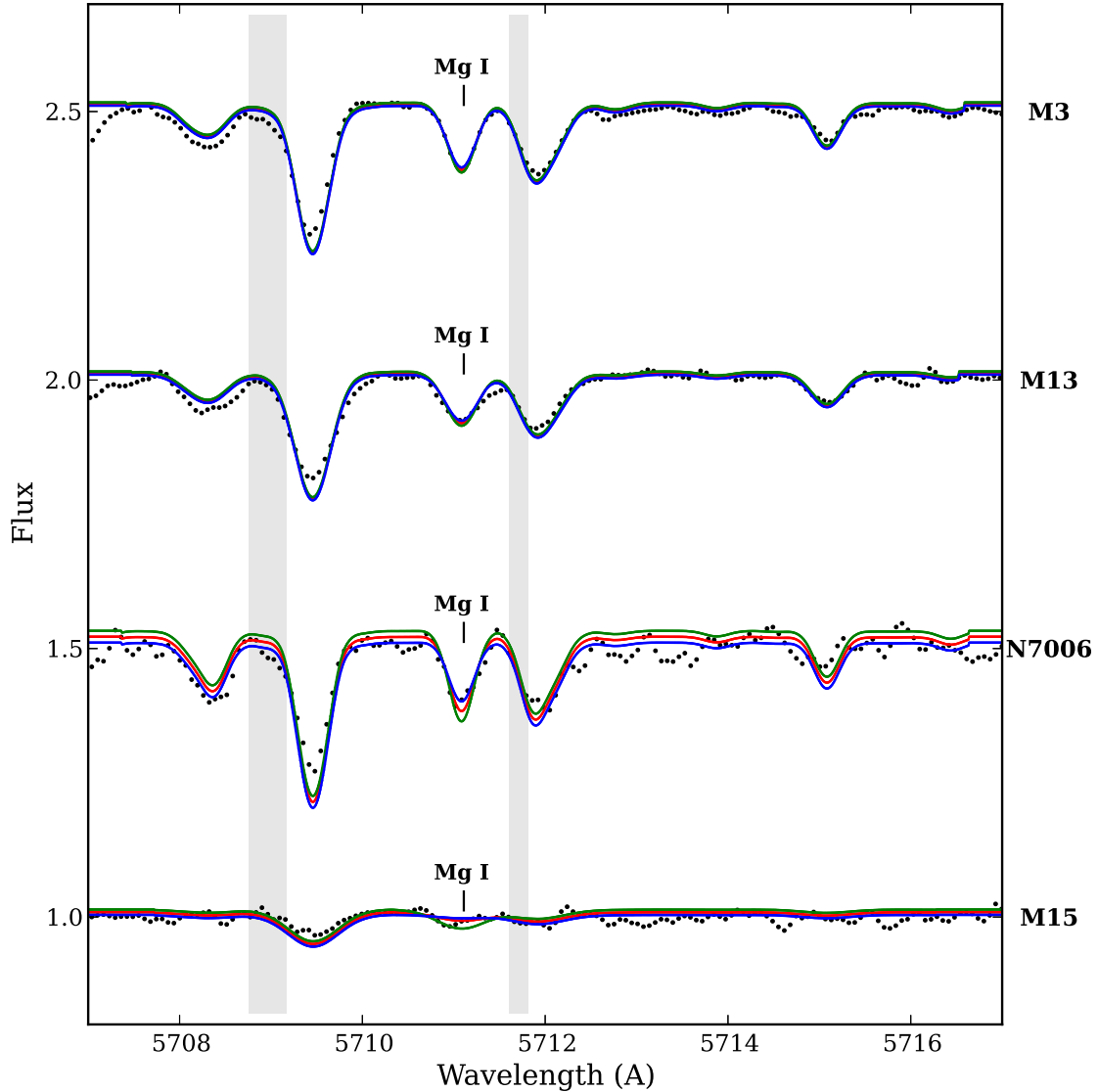


Figure 12. Spectrum syntheses of the 5711 Å Mg I line in M3, M13, NGC 7006, and M15. Lines are as in Figure 6.

be adopted. However, if the carbon abundance is treated as a free parameter, and is determined by fitting the CN lines in the region (the magenta line in Figure 17), the systematic errors in abundance can be reduced.

The Final Line List spectrum synthesis abundances are shown in Table 10, along with the literature averages. The Solar value is slightly lower than the Asplund et al. (2009) value. The Arcturus abundance again agrees with the average literature value. The 47 Tuc ILS [Eu/Fe] value is higher than MB08's [Eu/Fe] = 0.04, which is based on an equivalent width analysis with the same spectrum; measurements of this weak line may be more difficult than originally realized. The syntheses presented here show that the width of the synthesized line is wider than the observed feature

(see Figure 18), indicating that noise may have distorted the shape of the Eu II line. In this case, the spectrum syntheses, with a fixed FWHM broadening parameter, will do a better job of fitting the true line profile.

The IL Eu abundance in 47 Tuc is slightly higher than the average literature value, though the values do agree within the errors. The average literature [Eu/Fe] abundance in Pritzl et al. (2005) is based on the abundances of 5 giants, 8 subgiants, and 3 turnoff stars, whose abundances range from $-0.39 \lesssim [\text{Eu}/\text{Fe}] \lesssim +0.44$. The ILS abundance falls at the upper end of this observed range, suggesting that the Eu-enhanced stars are dominating the ILS Eu II line strength.

Thus, the precision of the abundance from the weak Eu II line

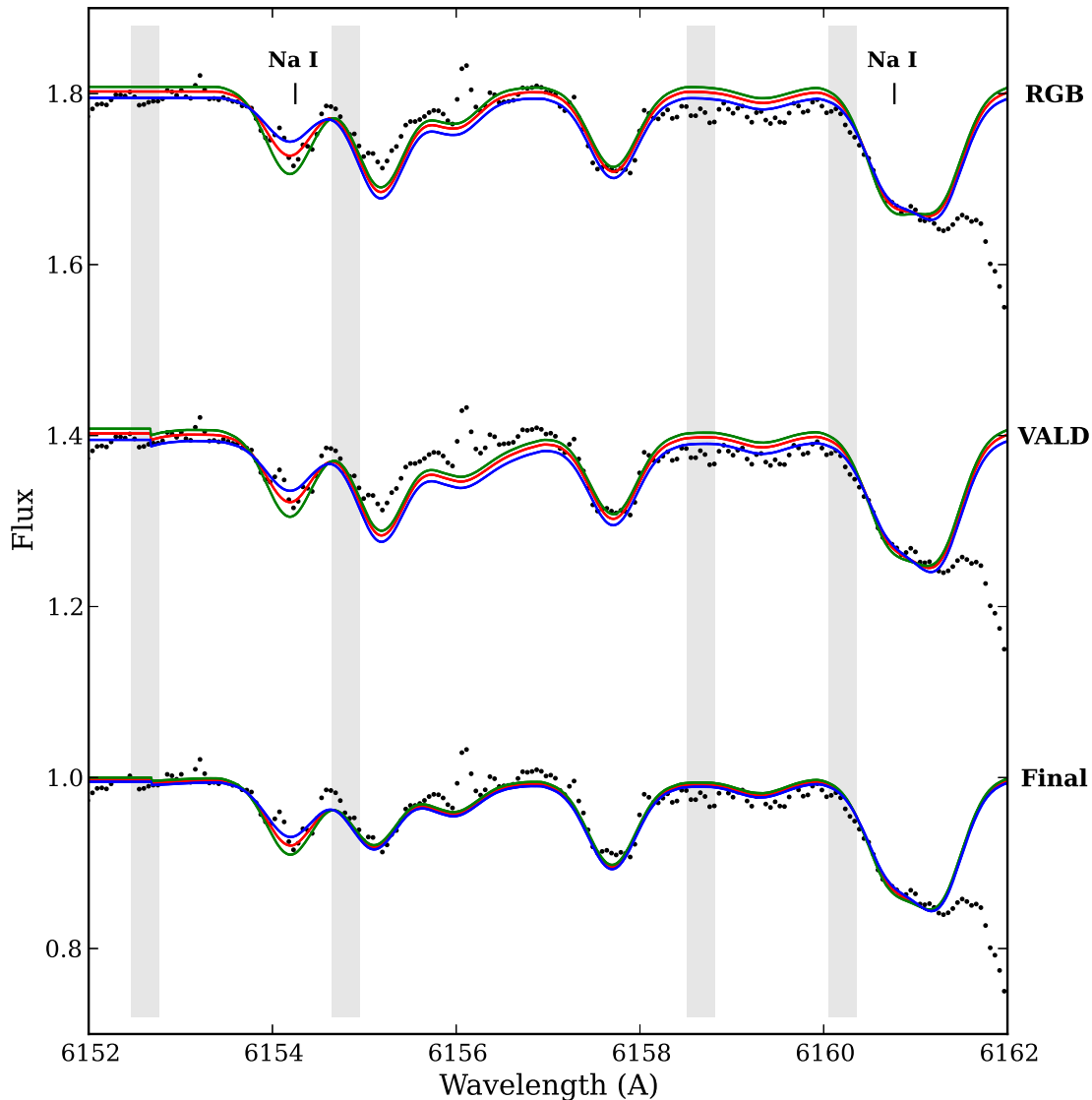


Figure 13. Spectrum syntheses of the 6154/6160 Å Na I lines in 47 Tuc, with the Minimal, VALD, and Final Line Lists. Lines are as in Figure 6.

has significantly improved with the use of the Final Line List, with the error decreasing to 0.10 from 0.18 and 0.15 for the Minimal and VALD Lists, respectively. The spectrum synthesis technique has also improved the accuracy of the derived abundance, as compared to the EW analysis.

4.3.3 Eu in the Other GCs

The syntheses of the Eu II line in the ILS of the other GCs are shown in Figure 19, and the abundances are given in Table 10. The input carbon abundances is less important for these GCs, since the CN lines are weaker. Table 10 shows that these clusters are all enhanced in Eu, and that these enhancements are considerably

greater than the literature averages. However, these literature averages do not reflect the Eu variations that exist within the clusters. Roederer (2011) has shown that large Eu dispersions are present in many Galactic GCs, including M3 ($0.4 \lesssim [\text{Eu}/\text{Fe}] \lesssim 0.8$), M13 ($0.2 \lesssim [\text{Eu}/\text{Fe}] \lesssim 1.0$), and M15 ($0.2 \lesssim [\text{Eu}/\text{Fe}] \lesssim 2.2$). NGC 7006 does not show a significant dispersion in Eu ($0.30 \lesssim [\text{Eu}/\text{Fe}] \lesssim +0.44$) but these abundances are based on observations of only six giants (Kraft et al. 1998). All of the integrated light synthesis-based abundances fall at the upper end of the literature ranges, again suggesting that the ILS-derived abundance is dominated by the most Eu-rich stars in the GCs.

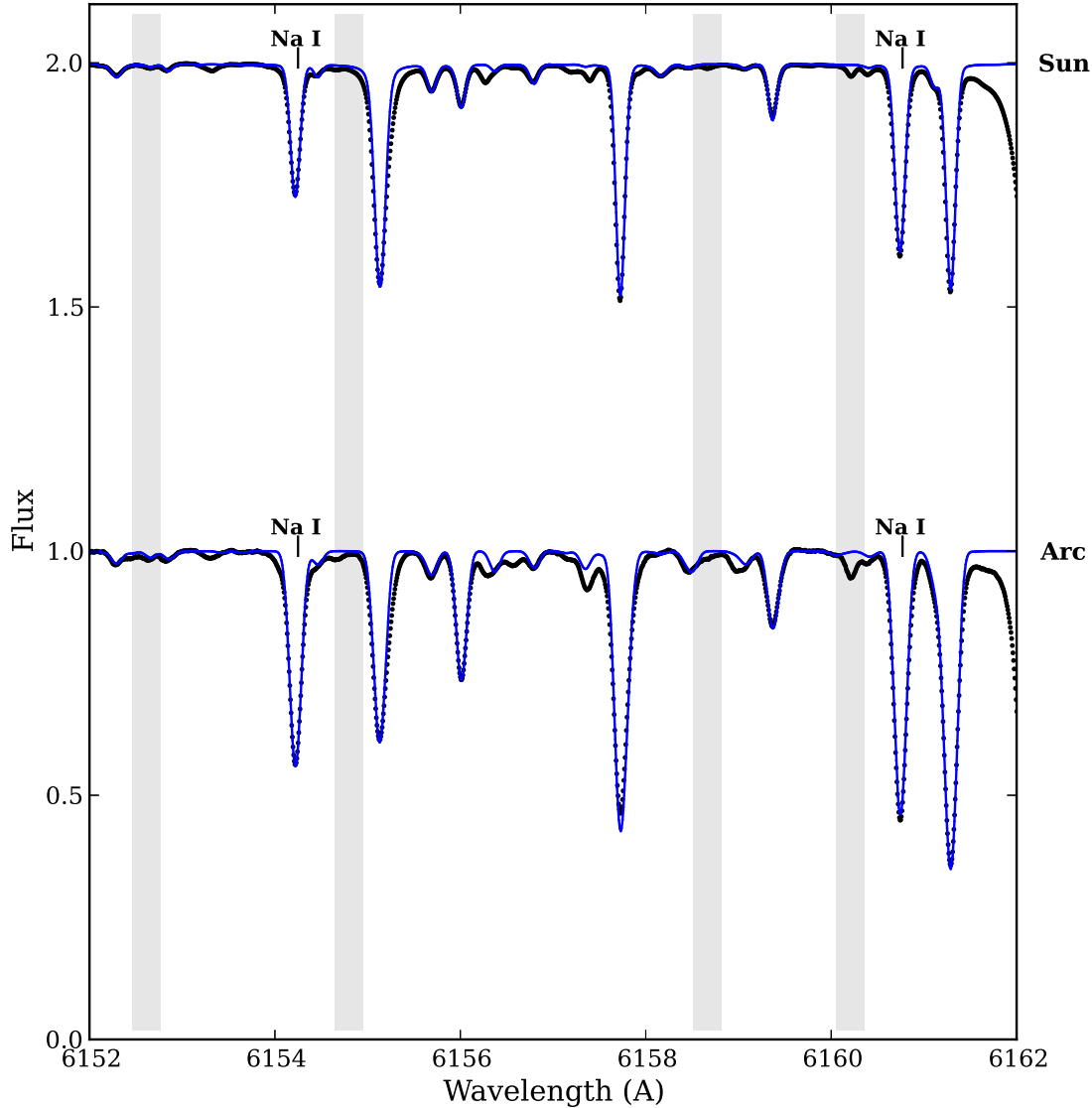


Figure 14. Spectrum syntheses of the 6154/6160 Å Na I lines on the Solar and Arcturus spectra. Lines are as in Figure 6.

5 DISCUSSION

Section 4 presented spectrum syntheses of high-resolution ILS of the five Galactic GCs 47 Tuc, M3, M13, NGC 7006, and M15, clusters which cover a wide range in metallicity (from $[\text{Fe}/\text{H}] \approx -0.7$ to -2.4) and HB morphology. This Section presents a discussion of the important findings from these syntheses.

5.1 The Nature of Integrated Light Spectrum Syntheses

The results from Section 4 clearly show that determining abundances from spectrum syntheses of ILS is more difficult than with individual, resolved stars. The severe blends in an ILS make fitting individual lines and identifying the continuum level difficult.

Comparisons between the individual Solar/Arcturus spectra and the 47 Tuc ILS clearly show that 47 Tuc does not have “traditional” continuum regions (i.e. regions that are free of any spectral lines)—even the most featureless regions in the 47 Tuc spectrum are blends of continuum *and* weak absorption features. This is particularly evident in Figure 20, which shows syntheses of the 6154/6160 Å Na I lines in the 47 Tuc ILS; both the unbroadened and broadened (by the velocity dispersion and instrumental broadening) spectra are shown. In this crowded region, the broadened spectrum never reaches the continuum level of the unbroadened spectrum. Thus, even the basic step of fitting the continuum level requires some *a priori* knowledge of the weak lines that are involved in the blending, and the abundances of the elements that cause those spectral

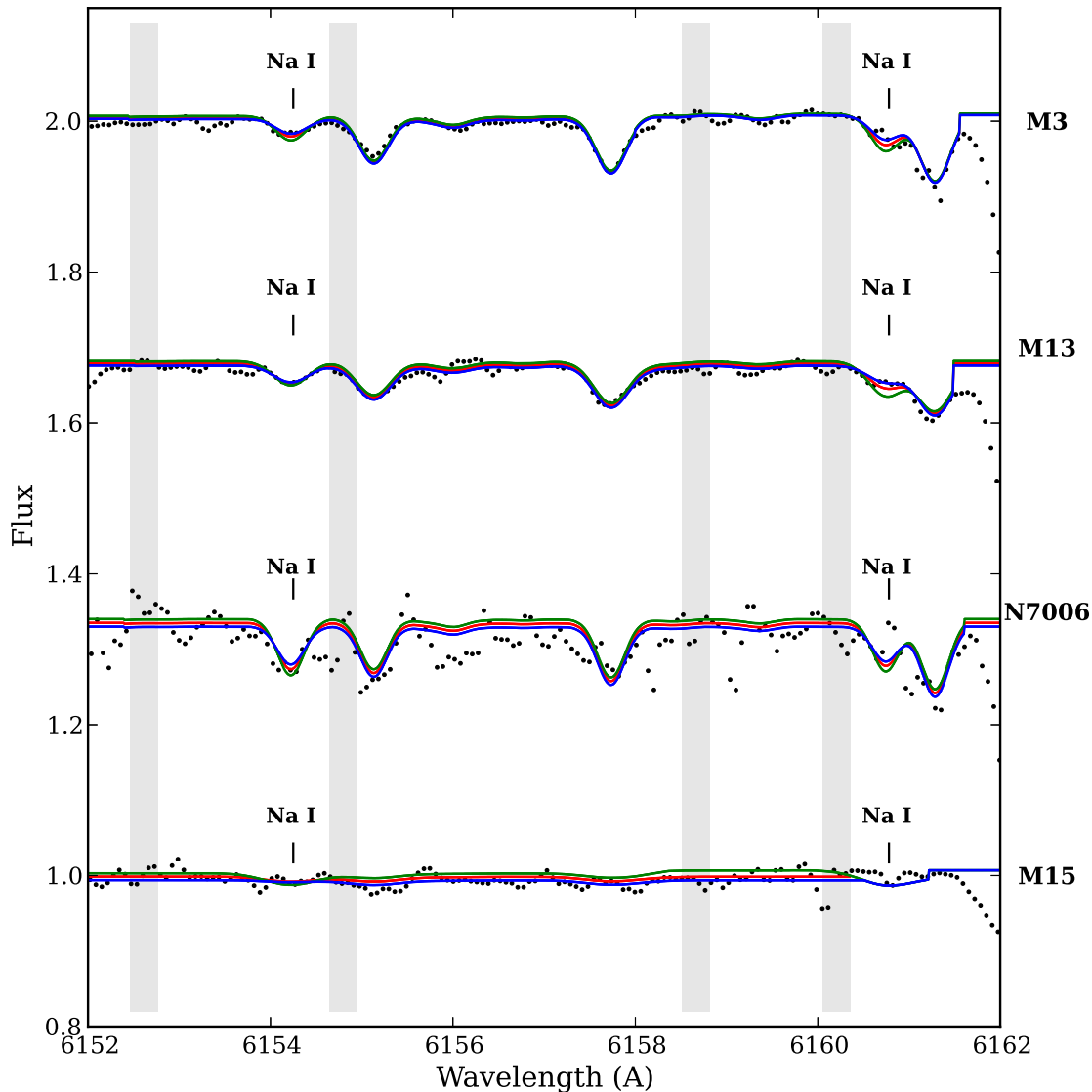


Figure 15. Spectrum syntheses of the 6154/6160 Å Na I lines on the M3, M13, NGC 7006, and M15 spectra. Lines are as in Figure 6. The 6160 Å line provides only an upper limit in M15.

lines. This once again illustrates the importance of having a complete and calibrated input line list.

Despite this concern, the uncertainties in continuum placement introduced by blended weak features may not be significant in all cases. The target GCs are all more metal-poor than the Sun and Arcturus, suggesting that fewer spectral lines are present throughout the GC spectra. The cluster velocity dispersion, which blends the lines together, also makes the weak lines weaker. Even if the lines are present and are strong enough to influence the continuum, the lines in the Final Line List have been calibrated to the Sun and Arcturus, meaning that once the integrated light abundances of the elements with the most lines (e.g., Fe, Ca, Ti, and Ni) have been determined (e.g., through an EW analysis), the synthesized lines

should match the observed ones. Thus, the well-calibrated strong lines from these well-known elements may also be used to fit the continuum. Ultimately, however, this problem is unavoidable in integrated light spectrum syntheses, and continuum level uncertainty should be considered as an important source of uncertainty in the integrated light abundances.

5.2 Comparisons with Literature Abundances

As is clear from the abundances presented in Section 4, caution must be taken when comparing ILS abundances to average literature values. *The ILS abundances do not represent average cluster abundances.* The stellar contributions to an ILS are flux-weighted,

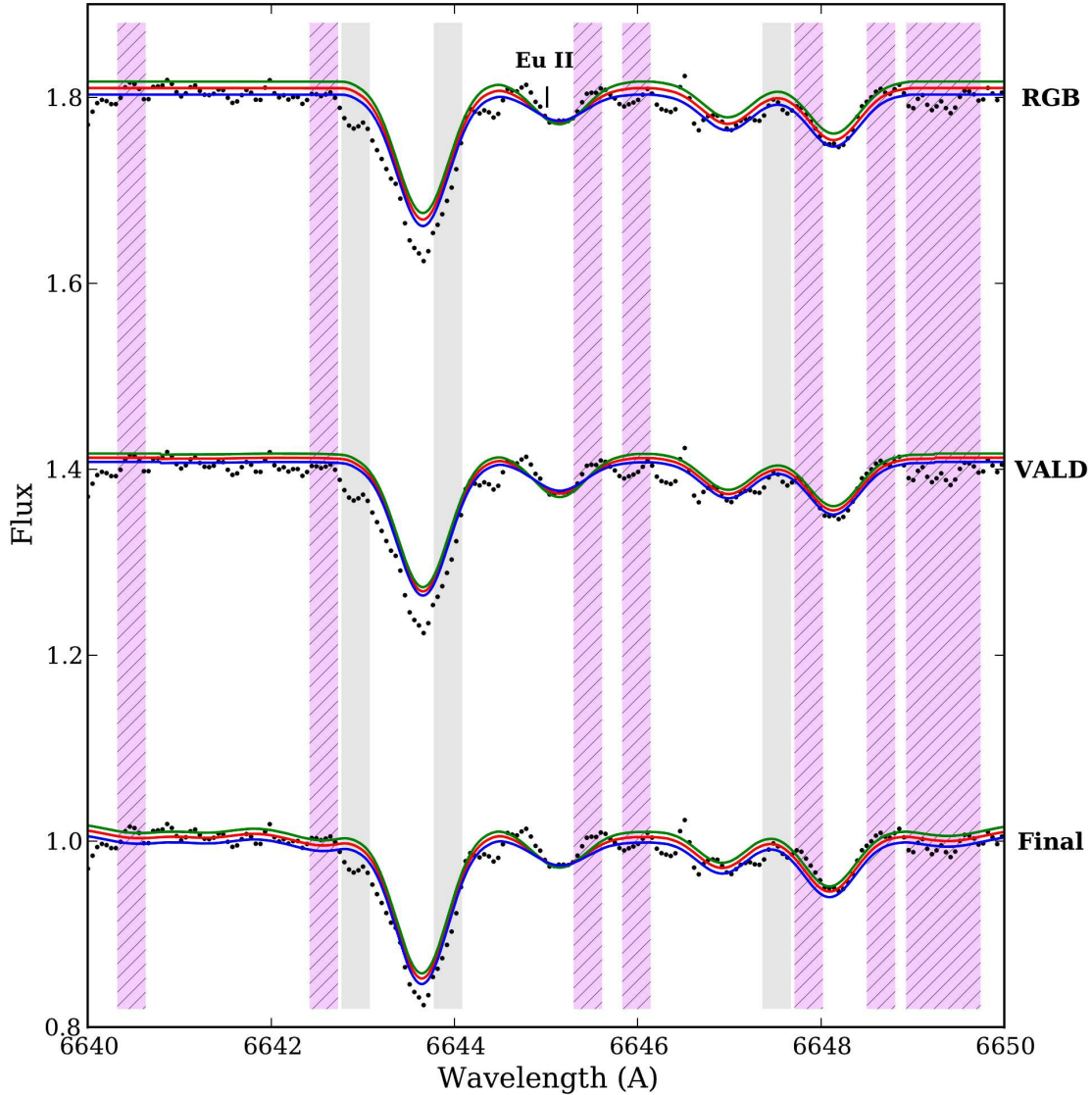


Figure 16. Spectrum syntheses of the 6645 Å Eu II line with the Minimal, VALD, and Final Line Lists. Lines are as in Figure 6.

meaning that the brightest RGB, AGB, and post-AGB stars contribute the most light to the observed spectrum (and therefore have more influence on a line’s shape and strength). Furthermore, the contributions to individual *line strengths* can also depend on line properties (e.g. ionization state, excitation potential, etc.; see Figure 9 in MB08). For elements that are not expected to vary significantly between stars in a given cluster (e.g. Fe), these effects will be unimportant (assuming the population is properly modeled). For elements that *are* expected to vary (such as Mg, Na, and Eu), the observed line strengths will also depend on the abundance spreads in the stars that dominated the light. The literature averages will also depend on the number and types of stars observed. It is important to consider these effects when comparing with literature abundances.

Flux-weighted literature averages may help with comparisons with ILS abundances, but this requires a reasonably complete sample of stars that are selected only from the observed regions.

For elements with star-to-star variations within a GC, such as Mg, Na, and Eu, it is therefore more instructive to consider the observed literature *ranges*, especially those observed among the brightest evolved stars that dominate the integrated light. These ranges will reflect any star-to-star abundance variations, whether due to effects that may occur up the RGB (e.g. mixing, Korn et al. 2007) or as a result of separate populations throughout the cluster. With this caveat in mind, the ILABUNDS spectrum synthesis method presented here provides accurate abundances that fall within the ranges of literature abundances from individual stars.

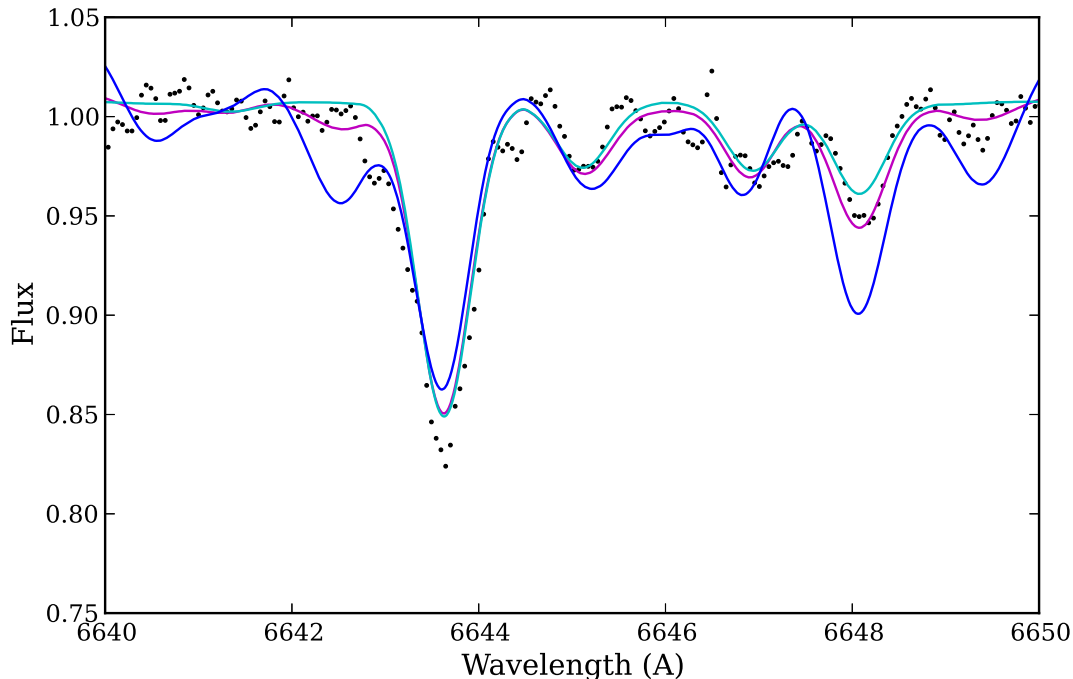


Figure 17. Syntheses of the region around the Eu II line in 47 Tuc with the CN molecules, and assuming a carbon isotopic ratio of $^{12}\text{C}/^{13}\text{C} = 9$. The cyan line assumes $[\text{C}/\text{Fe}] = -0.8$ and $[\text{N}/\text{Fe}] = 0.0$, typical of the C-enhanced stars in 47 Tuc, while the blue synthesis represents the C-deficient abundances, $[\text{C}/\text{Fe}] = 0.4$ and $[\text{N}/\text{Fe}] = 2.0$ (Briley et al. 2004). The syntheses have been vertically shifted to fit the continuum, and the Eu abundances were then altered to best fit the Eu II 6645 Å line. The Eu abundances differ by nearly 0.2 dex as a result of the differing input carbon abundances. The magenta line shows the synthesis with the best-fitting carbon abundance, as determined by fitting all the CN lines in the region; this case yields a Eu abundance similar to the CN-strong case.

5.3 The Chemical Signatures of Multiple Populations?

As standard Galactic GCs, 47 Tuc, M3, M13, NGC 7006, and M15 all show signs of multiple populations (under the definition of multiple populations as “synonymous with ‘multiple generations of stars’ that can be distinguished either from their spectra or from multiple sequences in the colour magnitude diagram;” Gratton et al. 2012). These multiple populations are often distinguished through star-to-star C, N, O, Na, Mg, and Al abundance variations (e.g. Carretta et al. 2009). These abundance variations are known to affect certain features in lower resolution ILS (e.g. Coelho et al. 2011 find that the Ca 4227, G4300, CN₁, CN₂, and NaD Lick indices are all affected by the second generation abundance differences). The high-resolution integrated light Na and Mg abundances presented here are therefore likely affected by these multiple populations within the GCs.

The abundance trends from the syntheses are generally qualitatively similar among the GCs. With the exception of M15, the GCs are all found to be Mg-enhanced in their integrated light, as compared to the Sun. Similarly, all GCs were found to be Na-enhanced. The magnitudes of these enhancements vary between the clusters. For example, 47 Tuc has the highest integrated light Mg enhancement and a moderate integrated light Na enhancement, while M15 shows Mg depletion and a much stronger Na enhancement. These findings qualitatively agree with the Na and Mg star-to-star variations in Galactic GCs, and suggest that in the observed regions, *stars from different populations may be dominating the integrated light in these clusters* (e.g. “normal” stars may dominate the 47 Tuc light, while more “second generation” Na-rich/Mg-

poor stars may dominate the M15 integrated light). This is likely a stochastic effect, and the integrated light abundances will likely depend on the area observed in the ILS. More theoretical work with multiple populations must be done in order to understand exactly how these effects will alter the integrated light abundances.

5.4 The Effects of Horizontal Branch Morphology

Metallicity variations alone cannot explain differences in HB morphologies in Galactic GCs (e.g. Sandage & Wildey 1967). Thus, there must be at least a *second parameter* governing HB morphology, such as age, although other factors are expected to contribute to differences in HB morphology (Dotter et al. 2010; Gratton et al. 2010). Because the physical causes behind HB morphology are not well understood, HB stars cannot be accurately modeled for all cluster types *a priori*. This means that for a given GC, the temperatures and surface gravities of the synthesized HB stars may not be accurate. In addition, uncertain physical processes (e.g. radiative levitation; Michaud et al. 2008) can lead to abundance anomalies in hot HB stars (e.g. Fe; Lovisi et al. 2012), which complicates their contributions to the ILS.¹⁵ Although HB stars do not contribute much of the optical light in Galactic GCs (Schiavon et al. 2002) and although HB morphology does not have a drastic effect on the integrated optical colors of GCs (Smith & Strader 2007), certain

¹⁵ However, these chemical variations in the hottest stars are unlikely to have any effect on the syntheses of the Mg I, Na I, and Eu II lines studied here, as discussed in Section 3.1.4.

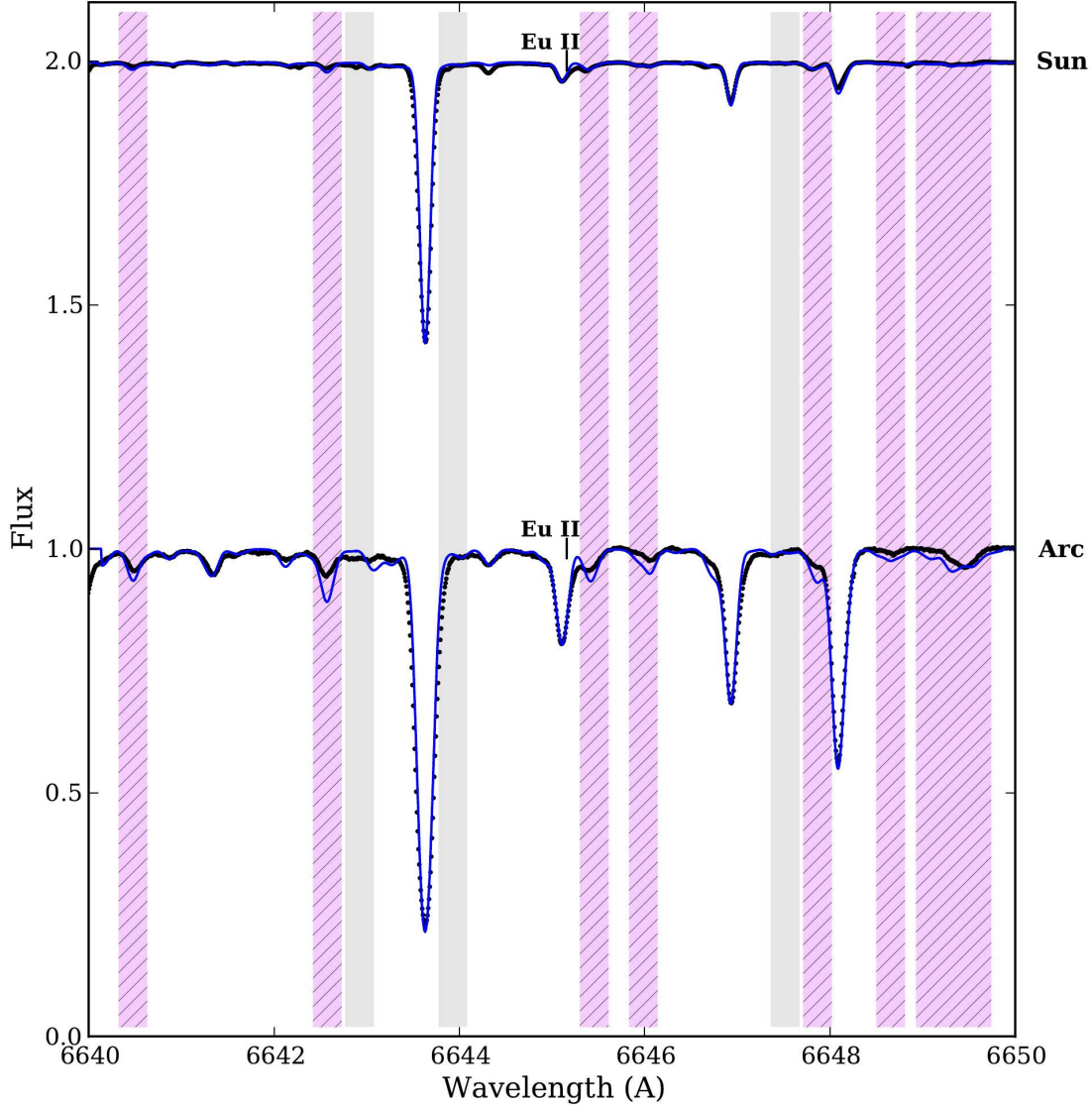


Figure 18. Spectrum syntheses of the 6645 Å Eu II line on the Solar and Arcturus spectra with the Final Line List. Lines are as in Figure 8.

spectral lines may be affected (i.e. those affected by hot stars, e.g. the Balmer lines, Schiavon et al. 2004; or partially ionized lines, MB08). Colucci et al. (2009) found that manually adding in blue HB stars did not significantly change the age and Fe estimates for M31 GCs, but the effects on spectrum syntheses have not yet been investigated.

The ILS and HST observations of the second parameter triad M3, M13, and NGC 7006 provide a unique opportunity to test the effects of HB morphology on synthetic spectra. If these Galactic clusters were unresolved, their HB morphologies would not be known *a priori*—the adopted models might synthesize HBs that are bluer or redder than the real HB. With resolved photometry, the HB morphology of one of these second parameter clusters, M3, is de-

liberately mis-modeled (using the HB photometry from the other second parameter clusters). The effects of an improperly modeled HB on the spectrum syntheses of Mg, Na, and Eu can then be tested directly. The effects of a purely red HB can also be investigated, by putting all the HB stars into the reddest HB box. In all cases the total number of HB stars is preserved.

The resulting abundance changes are shown in Table 11. The abundance differences are quite small, in all cases; in particular, the abundance differences between the syntheses with M3’s HB and NGC 7006’s HB are insignificant. The largest abundance differences occur for the synthesis of the 5528 Å Mg I line with the purely red HB, though the other lines show much smaller abundance differences with the reddest HB. In general, the differences

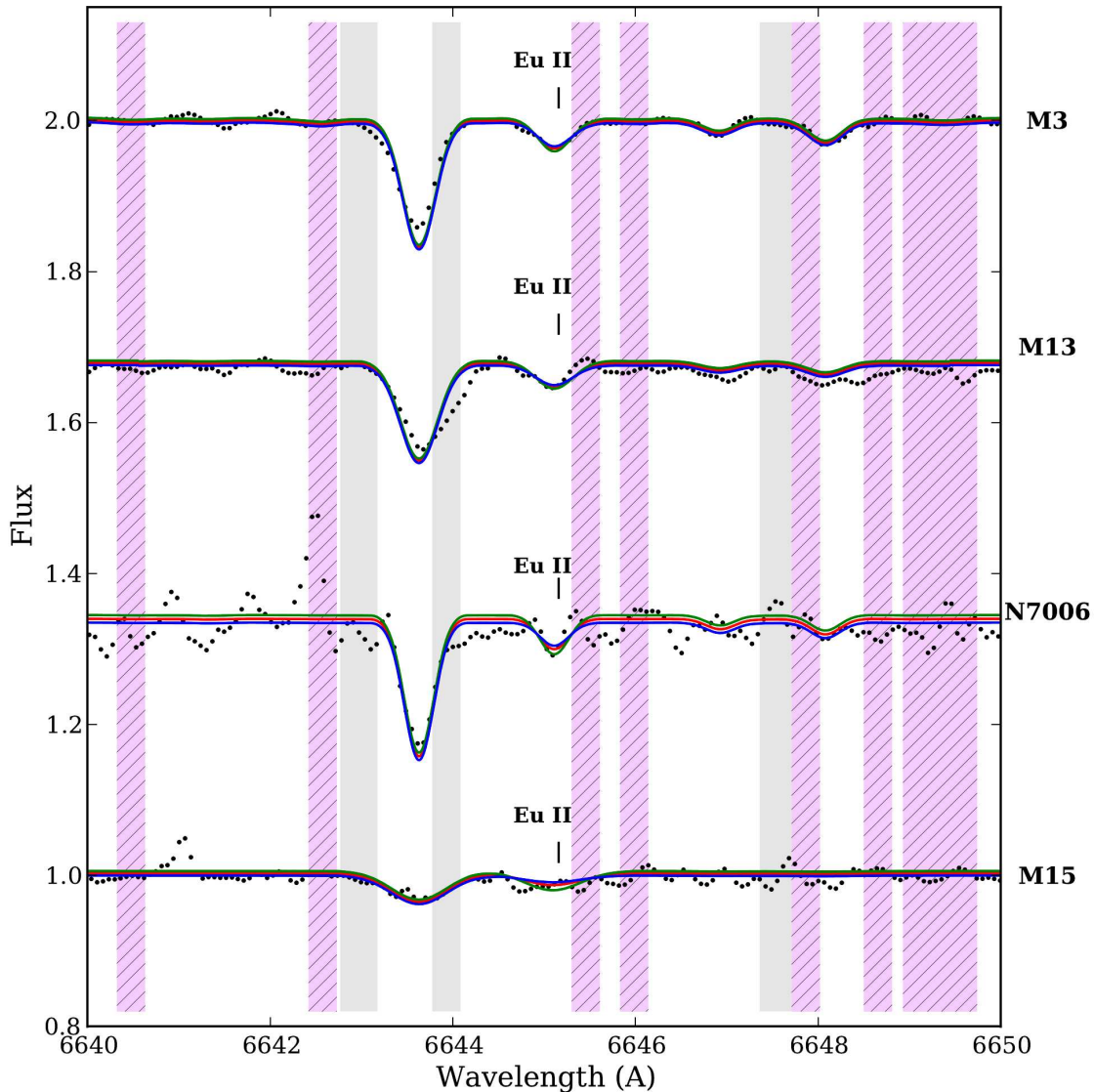


Figure 19. Spectrum syntheses of the 6645 Å Eu II line on the M3, M13, NGC 7006, and M15 ILS. Lines are as in Figure 8.

with a HB that is too blue are all insignificant (with $\Delta \log \epsilon \lesssim 0.03$). Though the resulting abundance changes are small, the effects are not isolated to the lines of interest. A different HB morphology affects lines throughout the spectrum, as shown in Figure 21. All lines in the region around the 5711 Å line, including the Fe lines, are affected by the HB morphology, which can affect the continuum placement. In this spectral region, the continuum changes are $< 1\%$, which causes a negligible error in abundance. However, this test shows that some spectral lines and regions are more sensitive to the HB morphology than others, even at red wavelengths, since the blue HB stars add continuum flux. At bluer wavelengths the blue HB stars are likely to have an even stronger effect.

6 CONCLUSIONS

This work has introduced a high resolution integrated light spectrum synthesis technique, and has applied the method to five Galactic globular clusters over a wide range of metallicities and HB morphologies. Previous high-resolution ILS analyses were either only equivalent width analyses (e.g. MB08) or adopted different spectrum syntheses methods (e.g. Colucci et al. 2009). The spectrum synthesis method introduced here is fully consistent with the MB08 equivalent width technique, and is capable of reproducing the integrated abundances of 47 Tuc, as derived from an equivalent width analysis.

In particular, this work has produced the following key findings:

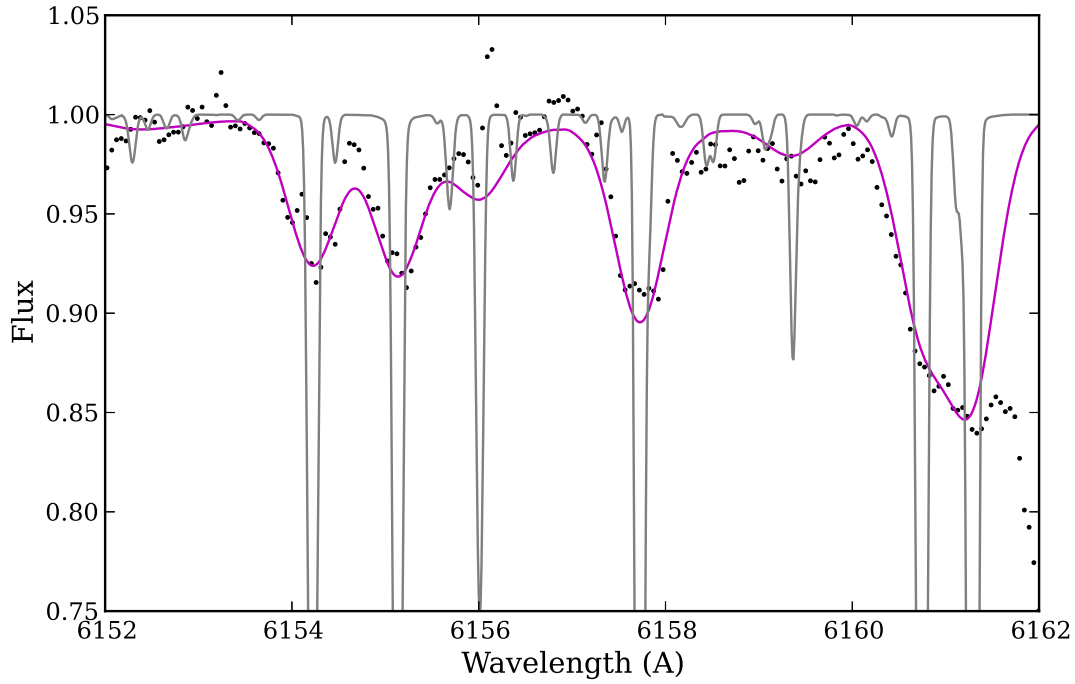


Figure 20. Syntheses of the Na I 6154/6160 Å doublet in the 47 Tuc spectrum. The magenta line shows the best-fitting abundance from Section 4.2.2. The grey line shows the same synthesis, *before it has been broadened by the velocity dispersion and instrumental broadening*. It is clear that the magenta line never fully reaches the continuum level of the grey synthesis, due to blending of the weak features.

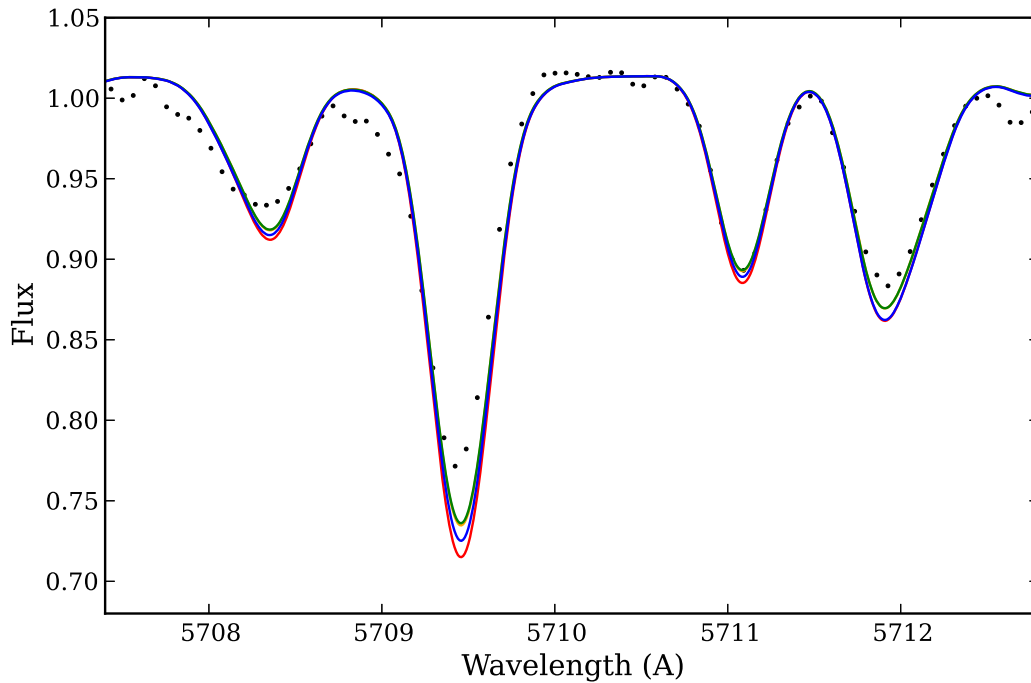


Figure 21. Spectrum syntheses of the 5711 Å Mg I line in the M3 ILS, with different HB morphologies. The green line shows M3's original intermediate HB morphology. The blue line shows M3's synthesis with M13's blue HB, the orange line shows M3's synthesis with NGC 7006's redder HB, and the red line shows M3 with a purely red HB.

Table 11. Abundance Changes with Various HB Morphologies

	M13's HB $\Delta \log \epsilon$	NGC 7006's HB $\Delta \log \epsilon$	Purely Red HB $\Delta \log \epsilon$
Mg 5528	-0.03	0.0	-0.06
Mg 5711	-0.02	0.0	-0.02
Na 6154	-0.03	0.0	-0.02
Eu 6645	-0.03	0.0	-0.12

The differences in abundance are with respect to the original synthesis, with M3's true HB stars. Three cases are considered: M3 with M13's HB, M3 with NGC 7006's HB, and M3 with a purely red HB. Lines throughout the region are affected by the HB morphology, which could influence continuum placement and line profile fitting.

- Spectrum syntheses of GC ILS can yield abundances with ~ 0.1 dex precision, comparable to the accuracy obtained with high quality spectral analyses of individual stars. To achieve this level of precision, attention must be given to the completeness of the input line list, which needs to be calibrated, e.g., to the Solar and Arcturus spectra. Molecular features do affect spectral lines of interest and the continuum determinations, and need to be included in the syntheses.

- The abundances determined here from the ILS of 47 Tuc, M3, M13, NGC 7006, and M15 fall within the abundance ranges in the literature from individual cluster member stars.

- The integrated light abundances may not represent the average cluster abundances in the literature, due to star-to-star abundance variations within each GC. The signatures of star-to-star abundance variations in Mg, Na, and Eu seem to be evident in the integrated light abundances of all the target GCs.

- HB morphology has only a negligible effect on the final Mg, Na, and Eu abundances from syntheses of the four spectral regions investigated here. Composition changes in the hottest stars, e.g., from radiative levitation, and rotational variations have a negligible effect on the abundances from these lines.

This work shows that high resolution ILS analyses can be used to determine precise elemental abundances in GCs, at least for certain lines of Mg, Na, and Eu, when the spectral line list is carefully considered. This method works over the observed range of metallicities and HB morphologies found in the target Galactic GCs.

ACKNOWLEDGMENTS

The authors thank the referee for helpful comments and suggestions. The authors thank R. Bernstein for the use of her 47 Tuc spectrum. CMS acknowledges funding from the Natural Sciences & Engineering Research Council (NSERC), Canada, via the Vanier CGS program. KAV acknowledges funding through the NSERC Discovery Grants program. The Hobby-Eberly Telescope (HET) is a joint project of the University of Texas at Austin, the Pennsylvania State University, Stanford University, Ludwig-Maximilians-Universität München, and Georg-August-Universität Göttingen. The HET is named in honor of its principal benefactors, William P. Hobby and Robert E. Eberly. The authors wish to thank the night operations staff of the HET for their assistance and expertise with these unusual observations.

REFERENCES

- Alpaslan, M. 2009, arXiv:0912.4755
- Alves-Brito, A., Barbuy, B., Ortolani, S. et al. 2005, *A&A*, 435, 657
- Anderson, J., Sarajedini, A., Bedin, L.R., et al. 2008, 135, 2055
- Asplund, M., Grevesse, N., Sauval, J.A., & Scott, P. 2009, *ARA&A*, 47, 481
- Barklem, P. S., Piskunov, N., & O'Mara, B. J. 2000, *A&AS*, 142, 467
- Barklem, P. S. & Asplund-Johansson, J. 2005, *A&A*, 435, 373
- Baumüller, D., Butler, K., & Gehren, T. 1998, *A&A*, 338, 637
- Behr, B.B., Cohen, J.G., & McCarthy, J.K. 2000, *ApJ*, 531, L37
- Behr, B.B. *ApJS*, 149, 67
- Bekki, K., Yahagi, H., Nagashima, M., & Forbes, D.A. 2008, *MNRAS*, 387, 1131
- Briley, M.M. 1997, *AJ*, 114, 1051
- Briley, M.M., Harbeck, D., Smith, G.H., & Grebel, E. 2004, *AJ*, 127, 1588
- Brodie, J.P. & Strader, J. 2006, *ARA&A*, 44, 193
- Brown, J.A. & Wallerstein, G. 1992, *AJ*, 104, 1818
- Burris, D.L., Pilachowski, C.A., Armandroff, T.E., et al. 2000, *ApJ*, 544, 302
- Cameron, S. 2009, PhD Thesis: The development of a detailed abundance analysis method intended for the integrated light spectra of extragalactic globular clusters (Michigan: University of Michigan)
- Carretta, E., Gratton, R.G., Bragaglia, A., Bonifacio, P., & Pasquini, L. 2004, *A&A*, 416, 925
- Carretta, E., Bragaglia, A., Gratton, R., & Lucatello, S. 2009, *A&A*, 505, 139
- Castelli, F. & Kurucz, R. L. 2004, in *IAU Symp. 210, Modelling of Stellar Atmospheres*, ed. N. Piskunov, W.W. Weiss, & D. F. Gray (San Francisco: ASP), A20
- Cayrel, R. 1988, in *IAU Symp. 132, The Impact of Very High S/N Spectroscopy on Stellar Physics*, ed. G. Cayrel de Strobel & M. Spite (Dordrecht: Kluwer), 345
- Chou, M.-Y., Majewski, S.T., Cunha, K., et al. 2010, *ApJ*, 720, 10
- Cohen, J. 2004, *AJ*, 127, 1545
- Cohen, J.G. & Melendez, J. 2005, *AJ*, 129, 303
- Coelho, P., Percival, S.M., & Salaris, M. 2011, *ApJ*, 734, 72
- Colucci, J.E., Bernstein, R.A., Cameron, S., McWilliam, A., & Cohen, J.G. 2009, *ApJ*, 704, 385
- Colucci, J.E., Bernstein, R.A., Cameron, S.A., & McWilliam, A. 2011a, *ApJ*, 735, 55
- Colucci, J.E. & Bernstein, R.A. 2011b, *EAS Pub. Ser.*, 48, 275
- Colucci, J.E., Bernstein, R.A., Cameron, S.A., & McWilliam, A. 2012, *ApJ*, 746, 29
- Dotter, A., Sarajedini, A., Anderson, J., et al. 2010, *ApJ*, 708, 698
- Dotter, A., Sarajedini, A., & Anderson, J. 2011, *ApJ*, 738, 74
- Freeman, K. & Bland-Hawthorn, J. 2002, *ARA&A*, 40, 487
- Fulbright, J.P., McWilliam, A., & Rich, R.M. 2006, *ApJ*, 636, 821
- Fulbright, J.P., McWilliam, A., & Rich, R.M. 2007, *ApJ*, 661, 1152
- Gilroy, K.K. & Brown, J.A. 1991, *ApJ*, 371, 578
- Gratton, R.G., Sneden, C., Carretta, E., & Bragaglia, A. 2000, *A&A*, 354, 169
- Gratton, R., Sneden, C., & Carretta, E. 2004, *ARA&A*, 42, 385
- Gratton, R., Carretta, E., Bragaglia, A., Lucatello, S., & D'Orazi, V. 2010, *A&A*, 517, A81
- Gratton, R.G., Carretta, E., & Bragaglia, A. 2012, *ARA&A*, 20, 50

- Gratton, R.G., Lucatello, S., Sollima, A. et al. 2013, *A&A*, 549, 41
- Guhathakurta, P., Yanny, B., Schneider, D.P., & Bahcall, J.N. 1992, *AJ*, 104, 1790
- Harris, W.E. 1996, *AJ*, 112, 1487 (2010 edition)
- Harris, W.E. 2000, *Globular Cluster Systems*, Saas-Fee Lectures, Hinkle, K., Wallace, L., Livingston, W., Ayres, T., Harmer, D., & Valenti, J. 2003, in *The Future of Cool-Star Astrophysics: 12th Cambridge Workshop on Cool Stars, Stellar Systems, and the Sun (2001 July 30 - August 3)*, eds. A. Brown, G.M. Harper, and T.R. Ayres, (University of Colorado), 851
- Howell, J.H., Guhathakurta, P., & Gilliland, R.L. 2000, *PASP*, 112, 1200
- Jasniewicz, G., de Laverny, P., Parthasarathy, M., Lèbre, A., & Thévenin, F. 2004, *A&A*, 423, 353
- Koch, A. & McWilliam, A. 2008, *AJ*, 135, 1551
- Korn, A.J., Grundahl, F., Richard, O. et al. 2007, *ApJ*, 671, 402
- Kraft, R.P., Sneden, C., Langer, G.E., & Prosser, C.F. 1992, *AJ*, 104, 645
- Kraft, R.P., Sneden, C., Smith, G.H., Shetrone, M.D., & Fulbright, J. 1998, *AJ*, 115, 1500
- Kupka, F., Ryabchikova, T.A., Piskunov, N.E., Stempels, H.C., & Weiss, W.W. 2000, *Baltic Astronomy*, 9, 590
- Kurucz, R.L. 2005, *Mem. Soc. Astron. Italiana*, 8, 189
- Lambert, D.L. & Ries, L.M. 1981, *ApJ*, 248, 228
- Lawler, J.E., Wickliffe, M.E., den Hartog, E.A., & Sneden, C. 2001, *ApJ*, 563, 1075
- Lee, H.-C. & Worthey, G. 2005, *ApJS*, 160, 176
- Lind, K., Asplund, M., Barklem, P.S., & Belyaev, A.K. 2011, *A&A*, 528, 103
- Lovisi, L., Mucciarelli, A., Lanzoni, B. et al. 2012, *ApJ*, 754, 91
- Mackey, A.D. & van den Bergh, S. 2005, *MNRAS*, 360, 631
- Mashonkina, L.I., Shimanskiĭ, V.V., & Sakhbullin, N.A. 2000, *Astronomy Reports*, 44, 790
- Matteucci, F., Raiteri, C.M., Busson, M., Gallino, R., & Gratton, R. 1993, *A&A*, 272, 421
- McCall, M.L. 2004, *AJ*, 128, 2144
- McWilliam, A., Preston, G.W., Sneden, C., & Shtetman, S. 1995a, *AJ*, 109, 2736
- McWilliam, A., Preston, G.W., Sneden, C., & Searle, L. 1995b, 109, 2757
- McWilliam, A. & Bernstein, R. 2008, *ApJ*, 684, 326
- Michaud, G., Richer, J., & Richard, O. 2008, *ApJ*, 675, 1223
- Mishenina, T.V., Kovtyukh, V.V., Soubiran, C., Travaglio, C., & Busso, M. 2002, *A&A*, 396, 189
- Muratov, A.L. & Gnedin, O.Y. 2010, *ApJ*, 718, 1266
- Preston, G.W., Sneden, C., Thompson, I.B., Shtetman, S.A., & Burley, G.S. 2006, *AJ*, 132, 85
- Pritzl, B.J., Venn, K.A., & Irwin, M. 2005, *AJ*, 130, 2140
- Ramírez, I., & Melendez, J. 2005, *ApJ*, 626, 465
- Ramírez, I. & Allende Prieto, C. 2011, *ApJ*, 743, 135
- Ramsey, L.W., Adams, M.T., Barnes, T.G., et al. 1998, *Proc. SPIE*, 3352, 34
- Roederer, I.U. 2011, *ApJ*, 732, L17
- Sakari, C.M., Venn, K.A., Irwin, M., Aoki, W., Arimoto, N., & Dotter, A. 2011, *ApJ*, 740, 106
- Sandage, A. & Wildey, R. 1967, *ApJ*, 150, 469
- Sarajedini, A., Bedin, L.R., Chaboyer, B., et al. 2007, *AJ*, 133, 1658
- Sbordone, L., Bonifacio, P., Marconi, G., Buonanno, R., & Zaggia, S. 2005, *A&A*, 437, 905
- Schiavon, R.P., Faber, S.M., Castilho, B.V., & Rose, J.A. 2002, *ApJ*, 580, 850
- Schiavon, R.P., Rose, J.A., Courteau, S., & MacArthur, L.A. 2004, *ApJ*, 608, L33
- Shetrone, M.D. 1996, *AJ*, 112, 1517
- Shetrone, M.D., Cornell, M.E., Fowler, J.R., et al. 2007, *PASP*, 119, 556
- Smith, G.H. & Strader, J. 2007, *AN*, 328, 107
- Snedden, C. 1973, *ApJ*, 184, 839
- Snedden, C., Kraft, R.P., Shetrone, M.D., Smith, G.H., Langer, G.E., & Prosser, C.F. 1997, *AJ*, 114, 1964
- Snedden, C., Kraft, R.P., Guhathakurta, P., Peterson, R.C., & Fulbright, J. 2004, *AJ*, 127, 2162
- Sobeck, J.S., Kraft, R.P., Sneden, C. et al. 2011, *AJ*, 141, 175
- Stetson, P.B. & Pancino, E. 2008, *PASP*, 120, 1332
- Suda, T., Katsuta, Y., Yamada, S. et al. 2008, *PASJ*, 60, 1159
- Tolstoy, E., Hill, V., & Tosi, M. 2009, *ARA&A*, 47, 371
- Travaglio, C., Gallino, R., Arnone, E., Cowan, J., Jordan, F., & Sneden, C. 2004, *ApJ*, 601, 864
- Tull, R.G., 1998, *Proc. SPIE*, 3355, 387
- Venn, K.A., Shetrone, M.D., Irwin, M.J. et al. 2012, *ApJ*, 751, 102
- Worley, C.C., Cottrell, P.L., Freeman, K.C., & Wylie-de-Boer, E.C. 2009, *MNRAS*, 400, 1039
- Wylie, E.C., Cottrell, P.L., Sneden, C.A., & Lattanzio, J.C. 2006, *ApJ*, 649, 248
- Yong, D., Grundahl, F., Lambert, D.L., Nissen, P.E., & Shetrone, M.D. 2003, *A&A*, 402, 985
- Yong, D., Carney, B.W., & Teixeira de Almeida, M.L. 2005, *AJ*, 130, 597
- Yong, D., Aoki, W., & Lambert, D.L. 2006, *ApJ*, 638, 1018